

Loading and thermal behaviour of ZIF-8 metal-organic framework-inorganic glass composites

Ashleigh M. Chester^a, Celia Castillo-Blas^a, Roman Sajzew^b, Bruno P. Rodrigues^{b,c}, Giulio I. Lampronti^{a,d}, Adam F. Sapnik^a, Georgina P. Robertson^{a,e}, Matjaž Mazaj^f, Daniel J. M. Irving^e, Lothar Wondraczek^b, David A. Keen^g and Thomas D. Bennett^{a*}

^a*Department of Materials Science and Metallurgy, University of Cambridge, Cambridge, CB3 0FS, UK.*

^b*Otto Schott Institute of Materials Research, University of Jena, Fraunhoferstrasse 6, 07743 Jena, Germany.*

^c*Fraunhofer Institute for Applied Optics and Precision Engineering, Albert-Einstein-Str. 7, 07745, Jena, Germany.*

^d*Department of Earth Sciences, University of Cambridge, Cambridgeshire, CB2 3EQ, UK.*

^e*Diamond Light Source Ltd., Diamond House, Harwell Campus, Didcot, Oxfordshire OX11 0DE, UK.*

^f*National Institute of Chemistry, Hajdrihova 19, 1000 Ljubljana, Slovenia.*

^g*ISIS Facility, Rutherford Appleton Laboratory, Harwell Campus, Didcot, Oxfordshire OX11 0QX. UK.*

Email: tdb35@cam.ac.uk

Table of contents

1. List of Figures
2. ZIF-8 characterisation and controls
3. Inorganic glass characterisation
4. Composite characterisation
 - 4.1 PXRD analysis and optical microscopy
 - 4.2 FTIR spectroscopy
 - 4.3 Raman spectroscopy
 - 4.4 ^1H NMR spectroscopy
 - 4.5 SEM-EDX
 - 4.6 Thermal analysis: TGA/DSC
 - 4.7 PDF analysis
 - 4.8 CO₂ adsorption
 - 4.9 Air stability
 - 4.10 Maximum ZIF-8 loading
 - 4.11 VT-PXRD

1. List of Figures

Figure S1. SEM images of pristine ZIF-8.....	4
Figure S2. TGA of ZIF-8 and He pycnometry measurements of ZIF-8.....	4
Figure S3. Pawley refinement of experimental diffraction data of pristine ZIF-8.....	4
Figure S4. ^1H NMR spectrum of pristine ZIF-8.....	5
Figure S5. PXRD of pristine ZIF-8 and ZIF-8 under the reaction conditions	6
Figure S6. PXRD and TGA of the inorganic glass, $20\text{Na}_2\text{O}-10\text{NaCl}-70\text{P}_2\text{O}_5$	7
Figure S7. Full DSC up and down scans of inorganic glass $20\text{Na}_2\text{O}-10\text{NaCl}-70\text{P}_2\text{O}_5$	7
Figure S8. SEM image of inorganic glass powder.	8
Figure S9. SEM-EDS compositional analysis of the pristine inorganic glass	8
Figure S10. Optical images of the composites.....	10
Figure S11. PXRD patterns of the physical mixtures, pelletised physical mixtures and composites.....	10
Figure S12. Pawley refinement of the 10% ZIF-8 samples.....	11
Figure S13. Pawley refinement of the 20% ZIF-8 samples	13
Figure S14. Pawley refinement of the 30% ZIF-8 samples	15
Figure S15. Pawley refinement of the 40% ZIF-8 samples	17
Figure S16. FTIR spectra of pristine starting materials.....	19
Figure S17. Normalised FTIR spectra of the composites and starting materials.	19
Figure S18. FTIR spectra of the physical mixtures and composites.....	20
Figure S19. Raman spectra of the composites and ZIF-8.....	21
Figure S20. ^1H NMR spectrum of $(\text{ZIF-8})_{0.1}(\text{Inorganic})_{0.9}$ composite	22
Figure S21. Zoomed in region of ^1H spectrum of $(\text{ZIF-8})_{0.1}(\text{Inorganic})_{0.9}$ composite	22
Figure S22. ^1H NMR spectrum of $(\text{ZIF-8})_{0.2}(\text{Inorganic})_{0.8}$ composite	23
Figure S23. Zoomed in region of ^1H spectrum of the $(\text{ZIF-8})_{0.2}(\text{Inorganic})_{0.8}$	23
Figure S24. ^1H NMR spectrum of $(\text{ZIF-8})_{0.3}(\text{Inorganic})_{0.7}$ composite.....	24
Figure S25. ^1H NMR spectrum of $(\text{ZIF-8})_{0.4}(\text{Inorganic})_{0.6}$ composite	24
Figure S26. SEM images of the composites.....	25
Figure S27. SEM-EDX mapping of the $(\text{ZIF-8})_{0.1}(\text{Inorganic})_{0.9}$ composite	25
Figure S28. SEM-EDX mapping of the $(\text{ZIF-8})_{0.2}(\text{Inorganic})_{0.8}$ composite	26
Figure S29. SEM-EDX mapping of the $(\text{ZIF-8})_{0.3}(\text{Inorganic})_{0.7}$ composite	27
Figure S30. SEM-EDX mapping of the $(\text{ZIF-8})_{0.4}(\text{Inorganic})_{0.6}$ composite	27
Figure S31. TGA trace of $(\text{ZIF-8})(\text{Inorganic})(10/90)$ mixture.	28
Figure S32. TGA trace of $(\text{ZIF-8})(\text{Inorganic})(20/80)$ mixture.	28
Figure S33. TGA trace of $(\text{ZIF-8})(\text{Inorganic})(30/70)$ mixture.	29
Figure S34. TGA trace of $(\text{ZIF-8})(\text{Inorganic})(40/60)$ mixture.	29

Figure S35. TGA curves of the composites, starting materials and ZIF-8 controls.....	29
Figure S36. TGA trace of $(\text{ZIF-8})_{0.1}(\text{Inorganic})_{0.9}$ composite.....	30
Figure S37. TGA trace of $(\text{ZIF-8})_{0.2}(\text{Inorganic})_{0.8}$ composite.....	30
Figure S38. TGA trace of $(\text{ZIF-8})_{0.3}(\text{Inorganic})_{0.7}$ composite.....	30
Figure S39. TGA trace of $(\text{ZIF-8})_{0.4}(\text{Inorganic})_{0.6}$ composite.....	31
Figure S40. Full DSC up and down scans of the $(\text{ZIF-8})_{0.1}(\text{Inorganic})_{0.9}$ composite	31
Figure S41. Full DSC up and down scans of the $(\text{ZIF-8})_{0.2}(\text{Inorganic})_{0.8}$ composite	32
Figure S42. Full DSC up and down scans of the $(\text{ZIF-8})_{0.3}(\text{Inorganic})_{0.7}$ composite	32
Figure S43. Full DSC up and down scans of the $(\text{ZIF-8})_{0.4}(\text{Inorganic})_{0.6}$ composite	33
Figure S44. DSC upscans of the composites and inorganic glass	33
Figure S45. X-ray total scattering structure factor, $S(Q)$, of starting materials	34
Figure S46. X-ray total scattering structure factor, $S(Q)$, of the composites.....	34
Figure S47. X-ray pair distribution function $D(r)$ of pristine ZIF-8	35
Figure S48. X-ray pair distribution function $D(r)$ of pristine $20\text{Na}_2\text{O}-10\text{NaCl}-70\text{P}_2\text{O}_5$	35
Figure S49. X-ray pair distribution function $D(r)$ and MLR fit of the composites	36
Figure S50. Average Zn-P distances of crystalline zinc phosphates.....	36
Figure S51. Comparison of the $S(Q)$ and $D(r)$ plots of the $(\text{ZIF-8})_{0.1}(\text{Inorganic})_{0.9}$ before and after data adjustment and MLR fit of the <i>adjusted</i> $(\text{ZIF-8})_{0.1}(\text{Inorganic})_{0.9}$	37
Figure S52. CO_2 adsorption isotherms of the 10-40 ZIF-8 wt% composites and their parent materials.	38
Figure S53. Optical images of inorganic glass after and the $(\text{ZIF-8})_{0.4}(\text{Inorganic})_{0.6}$ composite after air exposure.....	39
Figure S54. PXRD of inorganic glass and $(\text{ZIF-8})_{0.4}(\text{Inorganic})_{0.6}$ composite after air exposure.....	39
Figure S55. DSC of inorganic glass after air exposure	40
Figure S56. DSC of $(\text{ZIF-8})_{0.4}(\text{Inorganic})_{0.6}$ composite after air exposure.....	40
Figure S57. Optical images of the 50-70 wt% composites.....	41
Figure S58. Pawley refinement of the 50-70 wt% composites.	42
Figure S59. PXRD patterns of the 50-70 wt% composites.....	43
Figure S60. CO_2 isotherms for the 50-70 wt% composites	44
Figure S61. TGA trace of the $(\text{ZIF-8})_{0.5}(\text{Inorganic})_{0.5}$ composite	45
Figure S62. VT-PXRD output data for the ZIF-8 control.	45
Figure S63. VT-PXRD output data for the $(\text{ZIF-8})_{0.5}(\text{Inorganic})_{0.5}$ composite.....	47
Figure S64. Refined lattice parameter and unit cell volume of the $(\text{ZIF-8})_{0.5}(\text{Inorganic})_{0.5}$ composite and ZIF-8 control.....	48

2. ZIF-8 characterisation

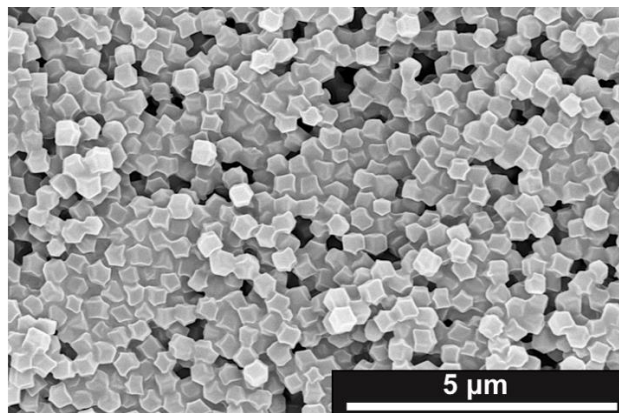


Figure S1. SEM images of pristine ZIF-8 using backscattered electron imaging mode with an acceleration voltage of 15 kV.

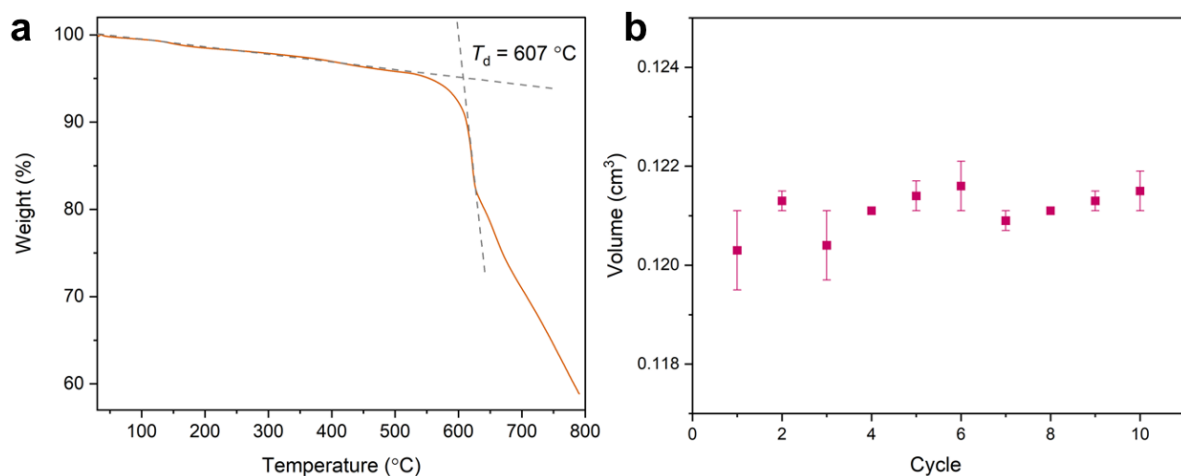


Figure S2 a. TGA of ZIF-8 using a heating rate of $10\text{ }^{\circ}\text{C min}^{-1}$ and **b.** Volume measurements recorded during He pycnometry measurements of ZIF-8. The density of ZIF-8 obtained was $1.59 \pm 0.006\text{ g cm}^{-3}$.

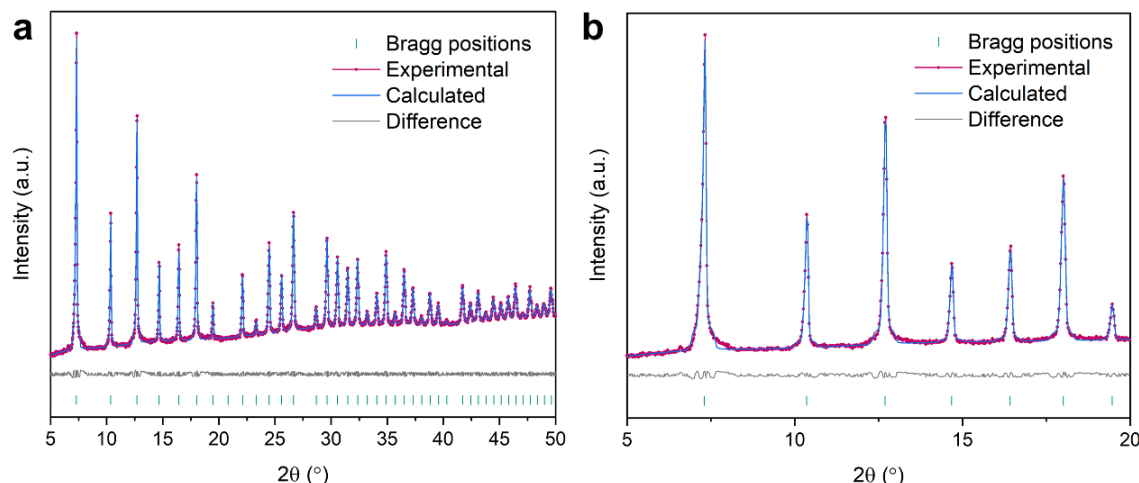


Figure S3. Experimental (pink dots), calculated (blue line), difference plot plot [(lobs-lcalc)] (grey line) and Bragg positions (green ticks) obtained from the Pawley refinement of experimental diffraction data of pristine ZIF-8 (space group: $I-43m$) for **a.** $2\theta = 5-2\theta = 5-50^{\circ}$ and **b.** $2\theta = 5-20^{\circ}$. Literature lattice parameter, $a = 16.8509(3)$.¹

Table S1. Pawley refinement details of pristine ZIF-8.

Sample	R_{wp}	Space group	Zero-point error	Profile parameters	Lattice parameter, a (Å)
ZIF-8	5.92%	$I-43m$	0.017(44)	U: -0.209(45) V: -0.074(13) W: 0.0064(8)	17.032(1)

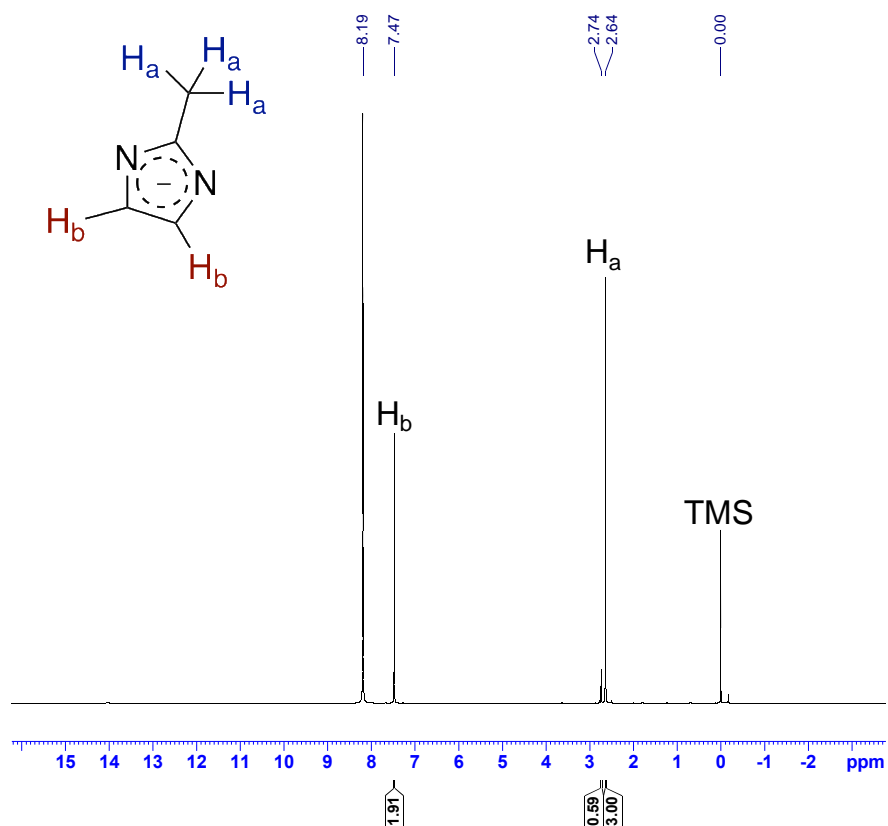


Figure S4. ^1H NMR spectrum of pristine ZIF-8. δ_{H} (500 MHz, DCI (35%)/D₂O: DMSO-d₆ (1:5), TMS) 8.19 (s, D₂O/DCI solvent), 7.47 (2H, s, H_b), 2.64, (3H, s, H_a), 0.00 (TMS).

ZIF-8 controls

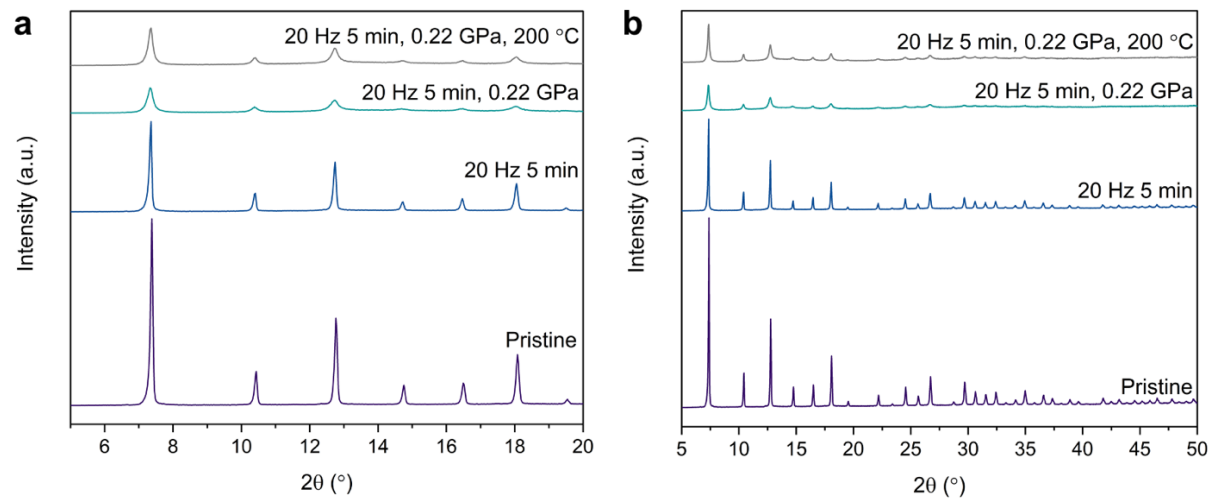


Figure S5. PXRD of pristine ZIF-8 and ZIF-8 under the reaction conditions in a range of **a.** $2\theta = 5-50^\circ$ and **b.** $2\theta = 5-20^\circ$.

3. Inorganic glass characterisation

The density obtained for the inorganic glass from He pycnometry, $20\text{Na}_2\text{O}\text{-}10\text{NaCl}\text{-}70\text{P}_2\text{O}_5$, $2.36 \pm 0.001 \text{ g cm}^{-3}$.

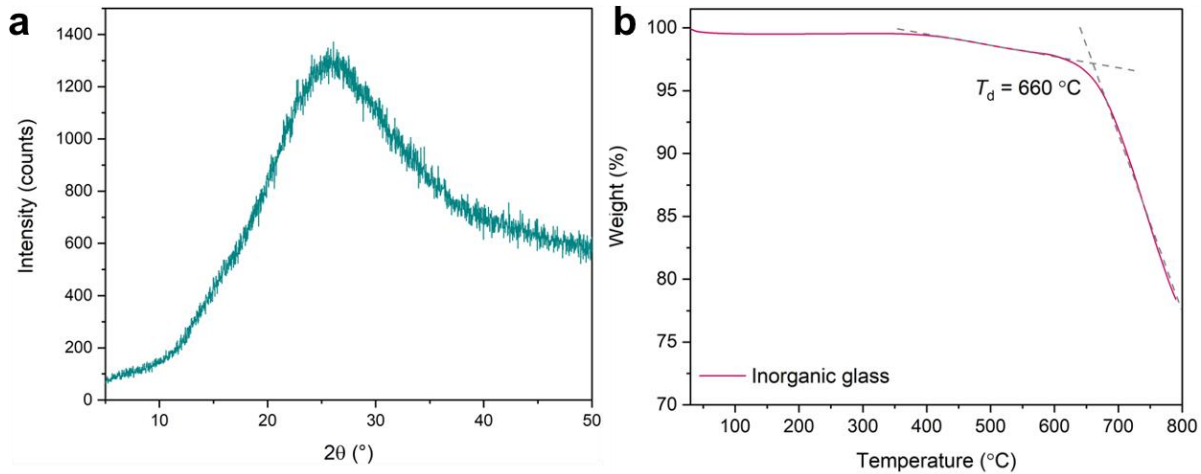


Figure S6. **a.** PXRD of the inorganic glass, $20\text{Na}_2\text{O}\text{-}10\text{NaCl}\text{-}70\text{P}_2\text{O}_5$ and **b.** TGA trace of the glass, showing a T_d of 660°C .

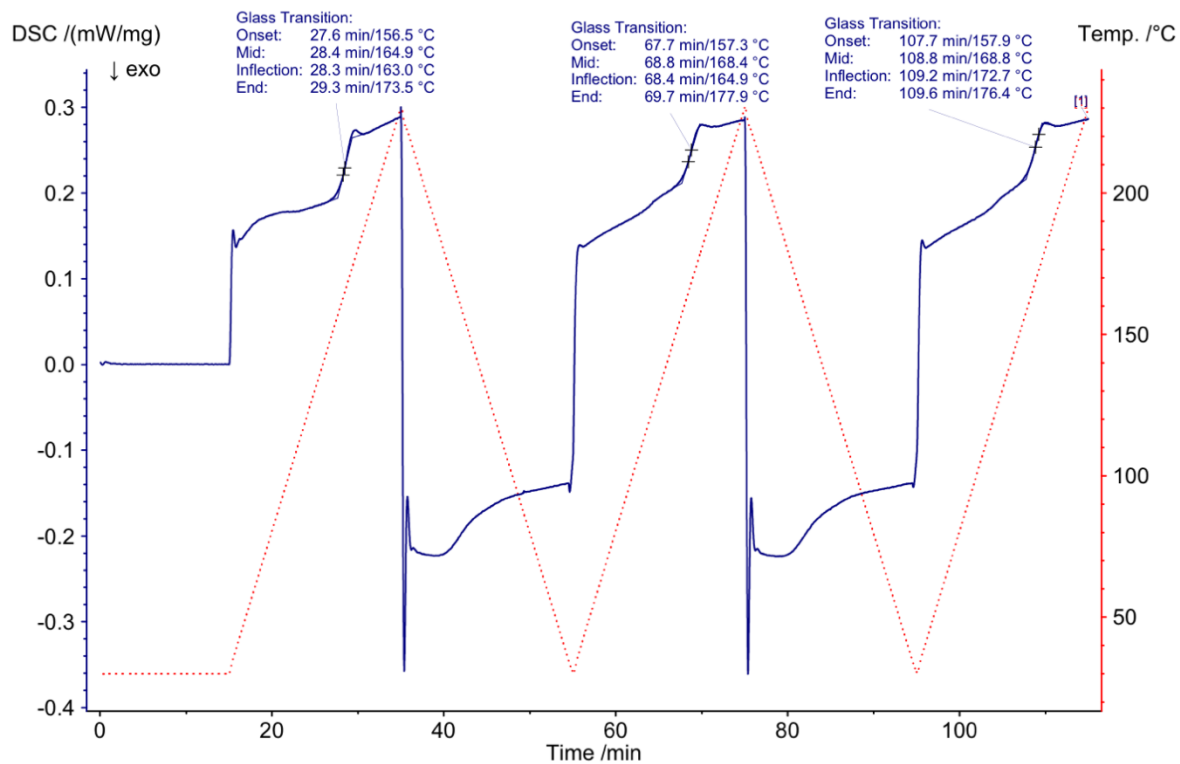


Figure S7. Full DSC up and down scans of inorganic glass $20\text{Na}_2\text{O}\text{-}10\text{NaCl}\text{-}70\text{P}_2\text{O}_5$ using a heating rate of $10^{\circ}\text{C min}^{-1}$ and a range of $30\text{-}450^{\circ}\text{C}$. A third upscan was taken to confirm the T_d .

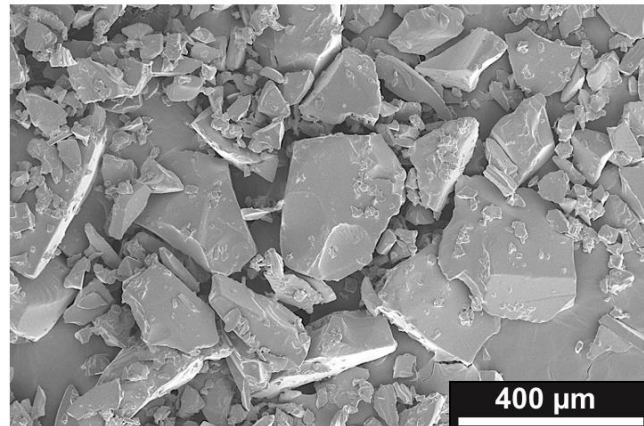


Figure S8. SEM image of inorganic glass powder, using secondary electron imaging mode and an acceleration voltage of 15 kV.

For SEM-EDS compositional analysis, five different areas (100-300 μm) of the inorganic glass were selected (**Figure S10**). Within each of these areas, multiple regions were selected (green rectangles) to determine the elemental homogeneity within the pristine glass. The amount of chlorine in the glass could not be accurately determined, likely because of its low content in the glass.

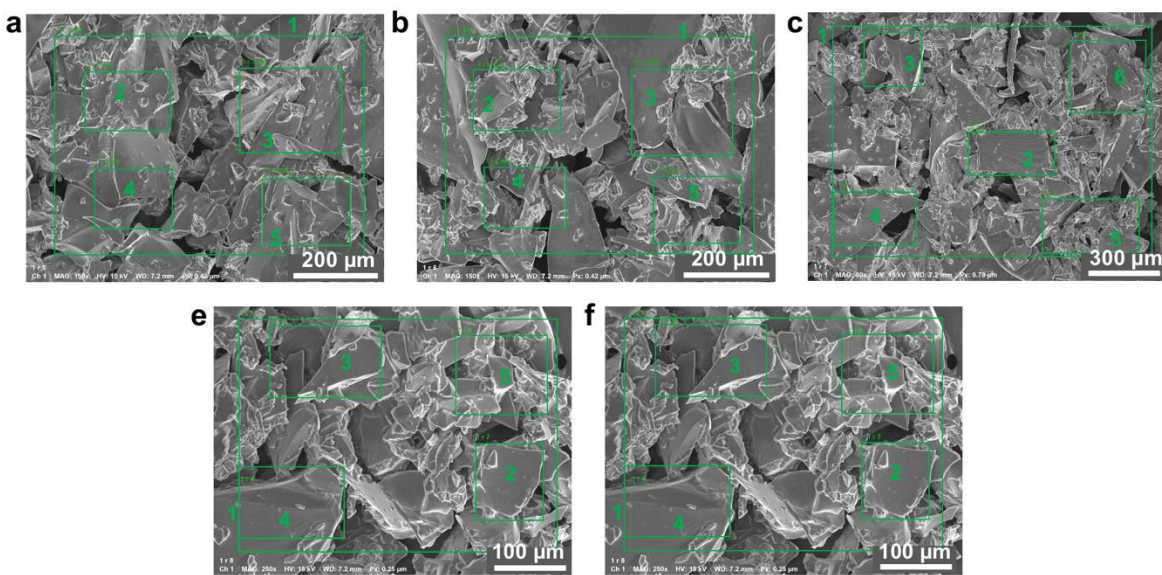


Figure S9. SEM-EDS compositional analysis of five regions of the pristine inorganic glass, $20\text{Na}_2\text{O}\text{-}10\text{NaCl}\text{-}70\text{P}_2\text{O}_5$, area 1 (a) to area 5 (e), with green rectangles representing regions analysed within these five areas.

Table S2. Elemental composition of 20Na₂O-10NaCl-70P₂O₅ determined by SEM-EDS.

	% O	% Na	% P	% Cl
Nominal	64.91	8.77	24.56	1.75
Area 1	67.70 ± 1.74	7.91 ± 0.53	24.39 ± 1.35	-
Area 2	68.11 ± 0.997	7.73 ± 0.51	24.15 ± 0.76	-
Area 3	67.69 ± 3.11	8.17 ± 1.07	24.13 ± 2.40	-
Area 4	67.91 ± 0.94	8.24 ± 0.28	23.84 ± 0.76	-
Area 5	69.26 ± 2.36	8.39 ± 1.83	22.34 ± 1.87	-
Average	68.14 ± 1.83	8.09 ± 0.85	23.77 ± 1.43	-

4. Composite characterisation

4.1 PXRD analysis and optical microscopy

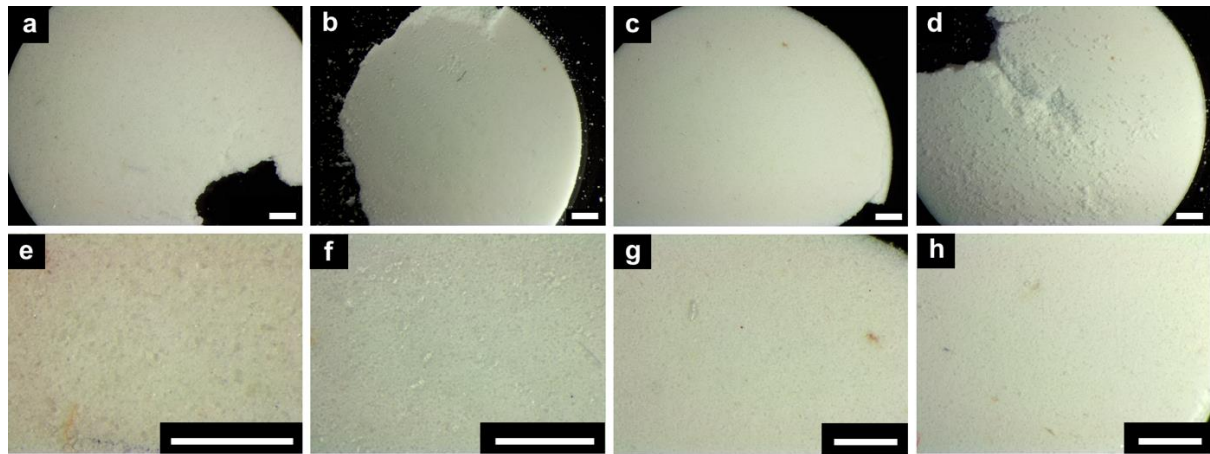


Figure S10. Optical images of the $(\text{ZIF-8})_{0.1}(\text{Inorganic})_{0.9}$ (a, e), $(\text{ZIF-8})_{0.2}(\text{Inorganic})_{0.8}$ (b, f), $(\text{ZIF-8})_{0.3}(\text{Inorganic})_{0.7}$ (c, g), and $(\text{ZIF-8})_{0.4}(\text{Inorganic})_{0.6}$ (d, h). Scale bar on all images is 1 mm.

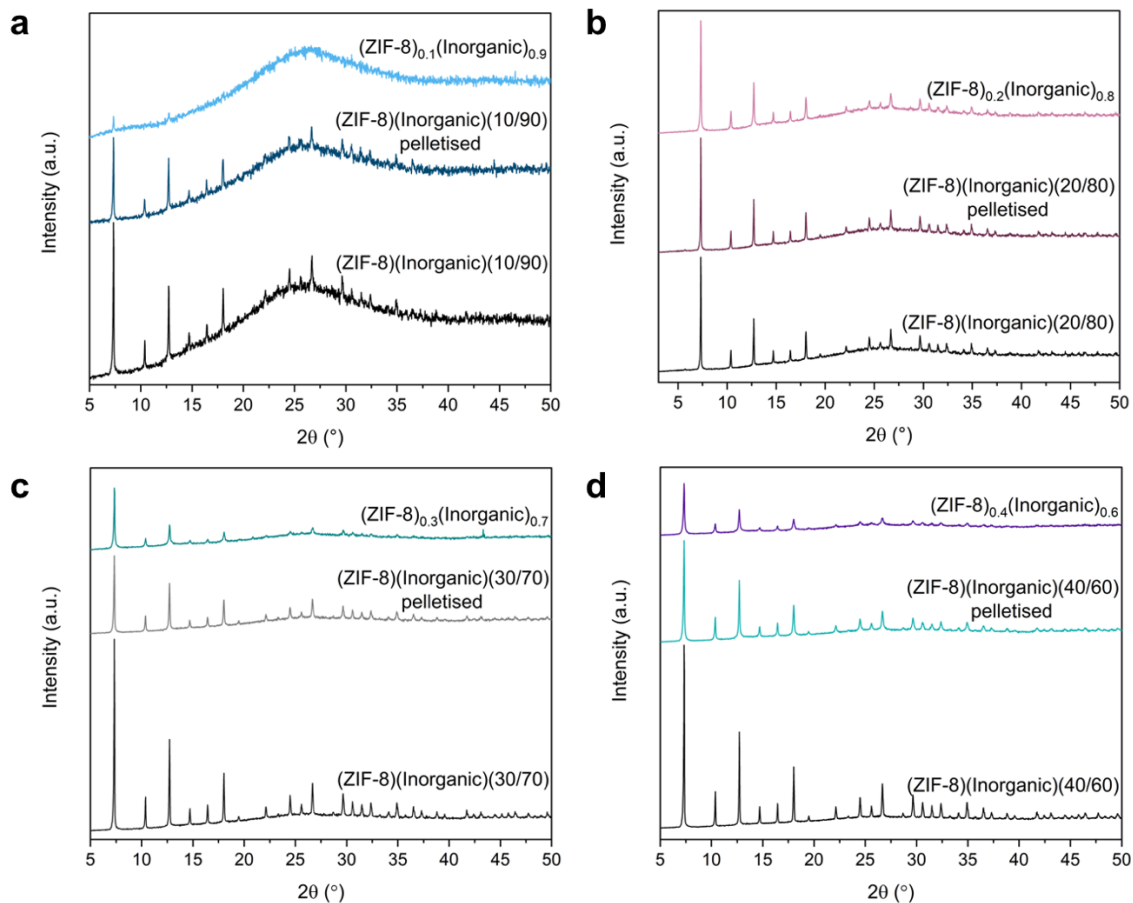


Figure S11. PXRD patterns of the physical mixtures, pelletised physical mixtures and composite post heating for **a.** $(\text{ZIF-8})_{0.1}(\text{Inorganic})_{0.9}$, **b.** $(\text{ZIF-8})_{0.2}(\text{Inorganic})_{0.8}$, **c.** $(\text{ZIF-8})_{0.3}(\text{Inorganic})_{0.7}$ and **d.** $(\text{ZIF-8})_{0.4}(\text{Inorganic})_{0.6}$. $(\text{ZIF-8})(\text{Inorganic})(X/Y)$ denotes the physical mixtures.

Initial parameters were obtained from the crystallographic information file previously reported for ZIF-8 for all refinements.

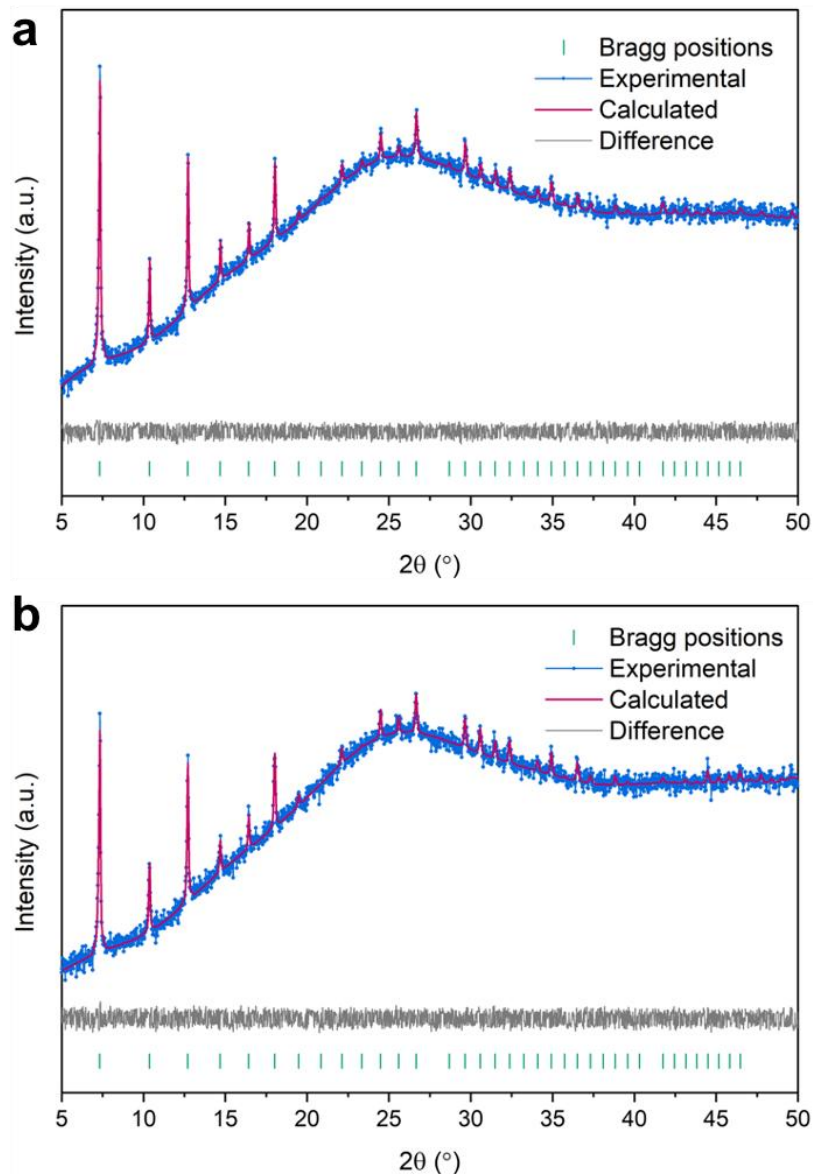


Figure S12. Pawley refinement of the 10% ZIF-8 sample, **a.** ((ZIF-8)(Inorganic)(10/90) mixture, **b.** Pelletised (ZIF-8)(Inorganic)(10/90) mixture.

Table S3. Pawley refinement details for 10% ZIF-8 samples. Space group for all samples was $I-43m$ and literature lattice parameter, $a = 16.8509(3)$ Å.¹ Experimental Lattice parameter of pristine ZIF-8 $a = 17.032(1)$ Å.

Sample	R_{wp}	Zero-point error	Profile parameters	Lattice parameter a (Å)
(ZIF-8)(Inorganic)(10/90)	4.02%	0.006(280)	U: -0.37(130) V: 0.19(29) W: -0.02(1)	17.020(6)
Pelletised (ZIF-8)(Inorganic)(10/90)	4.30%	0.02(30)	U: -0.23(17) V: 0.021(54) W: -0.0004(50)	17.031(8)
(ZIF-8) _{0.1} (Inorganic) _{0.9} *	N.A	N.A	N.A	N.A

*Refinement could not be carried out for the composite as only two Bragg peaks were observed post heating.

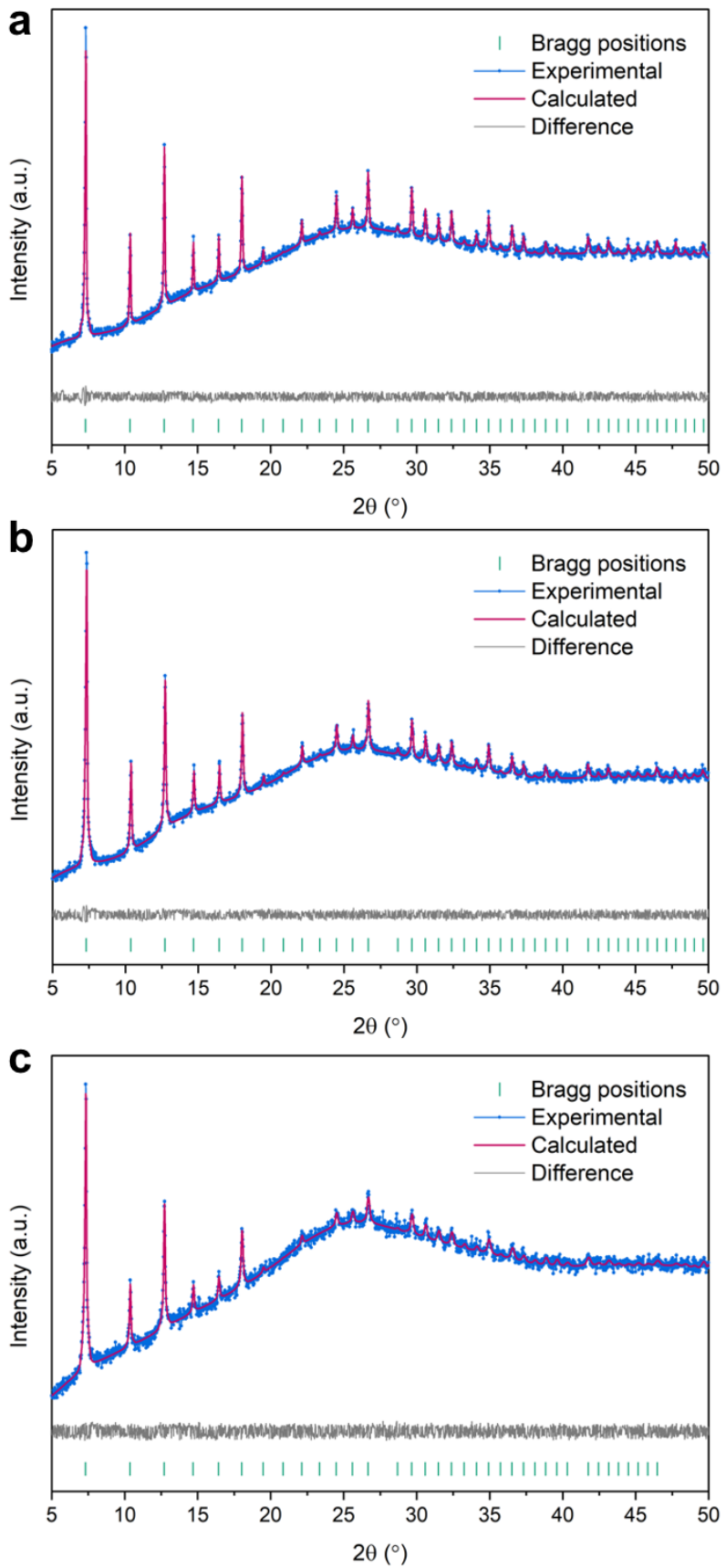


Figure S13. Pawley refinement of the 20% ZIF-8 sample, **a.** ((ZIF-8)(Inorganic)(20/80) mixture, **b.** Pelletised (ZIF-8)(Inorganic)(20/80) mixture and **c.** (ZIF-8)_{0.2}(Inorganic)_{0.8} composite.

Table S4. Pawley refinement details for 20% ZIF-8 samples. Space group for all samples was $I-43m$ and literature lattice parameter, $a = 16.8509(3)$ Å.¹ Experimental Lattice parameter of pristine ZIF-8 $a = 17.032(1)$ Å.

Sample	R_{wp}	Zero-point error	Profile parameters	Lattice parameter a (Å)
(ZIF-8)(Inorganic)(20/80)	4.10%	0.021(110)	U: 0.073(92) V: 0.0026(92) W: -0.0005(9)	17.024(3)
Pelletised (ZIF-8)(Inorganic)(20/80)	3.78%	0.025(150)	U: -0.15(48) V: -0.257(54) W: 0.0200(9)	17.028(3)
(ZIF-8) _{0.2} (Inorganic) _{0.8}	3.96%	0.018(370)	U: -0.999(5290) V: -0.26(110) W: 0.059(45)	17.016(8)

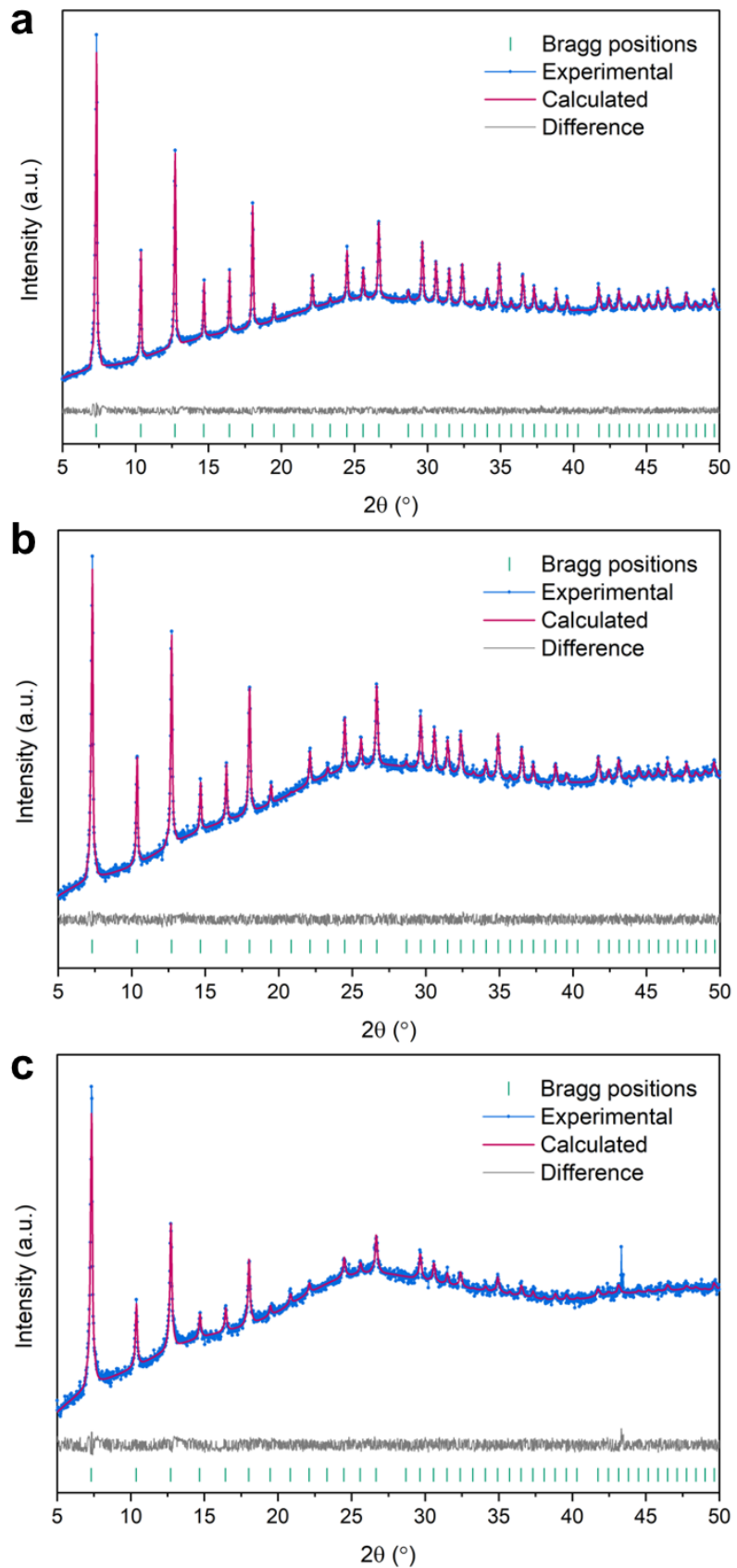


Figure S14. Pawley refinement of the 30% ZIF-8 sample, **a.** ((ZIF-8)(Inorganic)(30/70) mixture, **b.** Pelletised (ZIF-8)(Inorganic)(30/70) mixture and **c.** (ZIF-8)_{0.3}(Inorganic)_{0.7} composite.

Table S5. Pawley refinement details for 30% ZIF-8 samples. Space group for all samples was $I-43m$ and literature lattice parameter, $a = 16.8509(3)$ Å.¹ Experimental Lattice parameter of pristine ZIF-8 $a = 17.032(1)$ Å.

Sample	R_{wp}	Zero-point error	Profile parameters	Lattice parameter a (Å)
(ZIF-8)(Inorganic)(30/70)	4.17%	0.019(69)	U: 0.68(110) V: -0.053(37) W: 0.0032(22)	17.028(2)
Pelletised (ZIF-8)(Inorganic)(30/70)	3.69%	0.019(110)	U: 0.04(30) V: -0.142(95) W: 0.009(5)	17.029(3)
(ZIF-8) _{0.3} (Inorganic) _{0.7}	4.42%	0.021(330)	U: -0.41(140) V: -0.41(10) W: 0.026(9)	17.023(7)

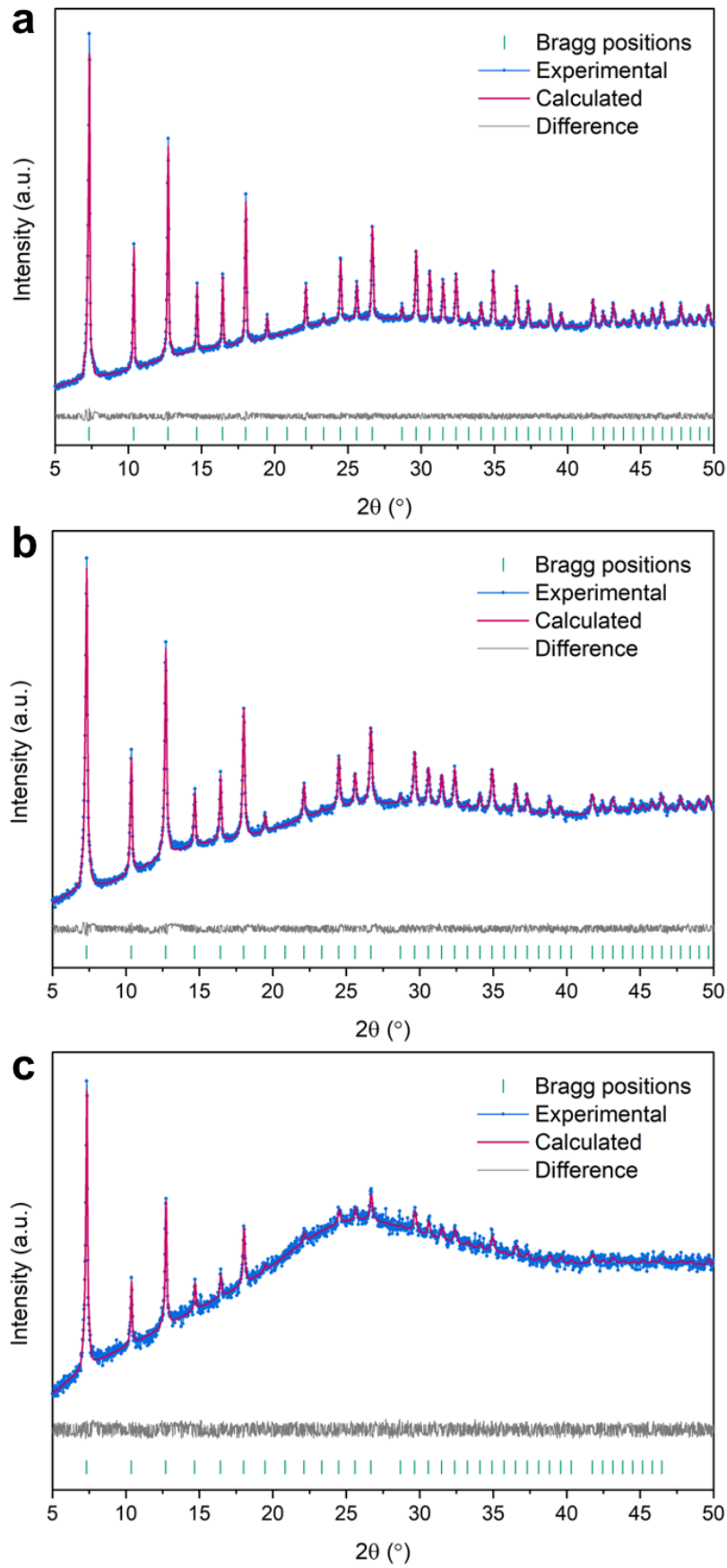
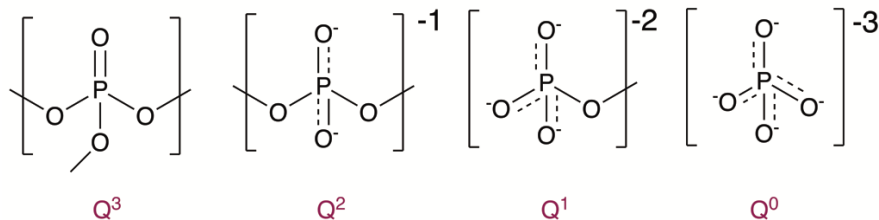


Figure S15. Pawley refinement of the 40% ZIF-8 sample, **a.** ((ZIF-8)(Inorganic)(40/60) mixture, **b.** Pelletised (ZIF-8)(Inorganic)(40/60) mixture and **c.** (ZIF-8)_{0.4}(Inorganic)_{0.6} composite.

Table S6. Pawley refinement details for 40% ZIF-8 samples. Space group for all samples was $I-43m$ and literature lattice parameter, $a = 16.8509(3)$ Å.¹ Experimental Lattice parameter of pristine ZIF-8 $a = 17.032(1)$ Å.

Sample	R_{wp}	Zero-point error	Profile parameters	Lattice parameter a (Å)
(ZIF-8)(Inorganic)(40/60)	4.38%	0.023(56)	U: -0.101(59) V: -0.032(14) W: 0.0024(6)	17.026(1)
Pelletised (ZIF-8)(Inorganic)(40/60)	3.83%	0.019(100)	U: -0.11(31) V: -0.2(1) W: 0.012(5)	17.023(2)
(ZIF-8) _{0.4} (Inorganic) _{0.6}	3.87%	0.021(220)	U: -0.39(53) V: -0.29(5) W: 0.020(5)	17.032(5)

4.2 FTIR spectroscopy



The inorganic glass' FTIR spectrum contains key bands at 1272 (P=O bond in Q^2/Q^3 units), 979 and 926 (P-O-P asymmetric stretch), 1090 (PO_3^{2-} asymmetric stretching) and 584 cm⁻¹ (P-O-P bending in and Q^2 and Q^3 units). The band at 1636 cm⁻¹ corresponds to P-OH and the broad band at 3429 cm⁻¹ corresponds to OH, indicating the glass has incorporated water into its structure.²

The ZIF-8 FTIR spectrum contains bands at 3129 and 2926 cm⁻¹ which correspond to C-H stretching mode of the methyl group in the 2-methylimidazole linker.^{3,4} The key C=N band can be observed at 1579 cm⁻¹, while bands at 1418 and 1304 cm⁻¹ are related to ring stretching of the 2-methylimidazole. Bands at 1143, 988 and 750 cm⁻¹ are from C-N stretching, while bands within the 600-800 cm⁻¹ are also associated with C-H stretching.

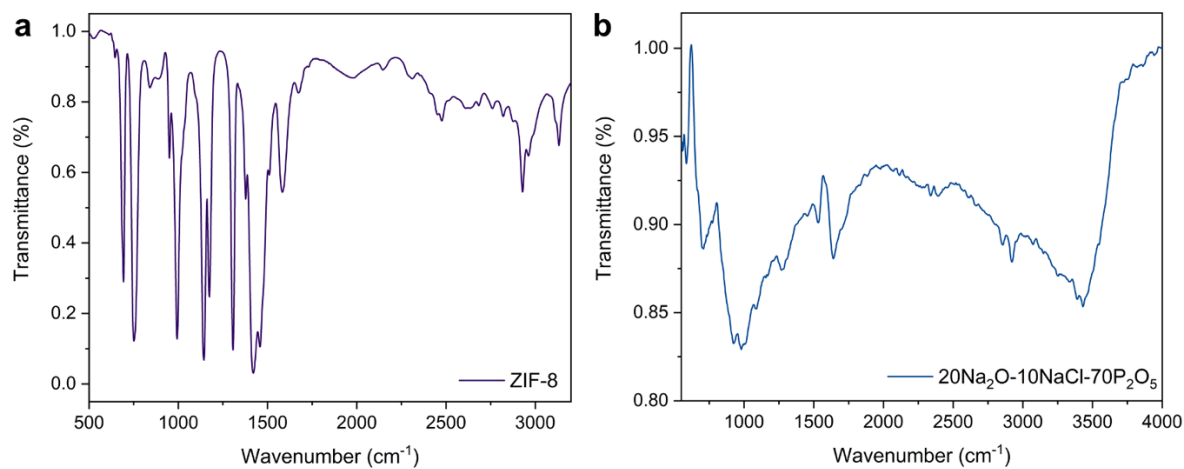


Figure S16. FTIR spectra of pristine **a.** ZIF-8 and **b.** Inorganic glass.

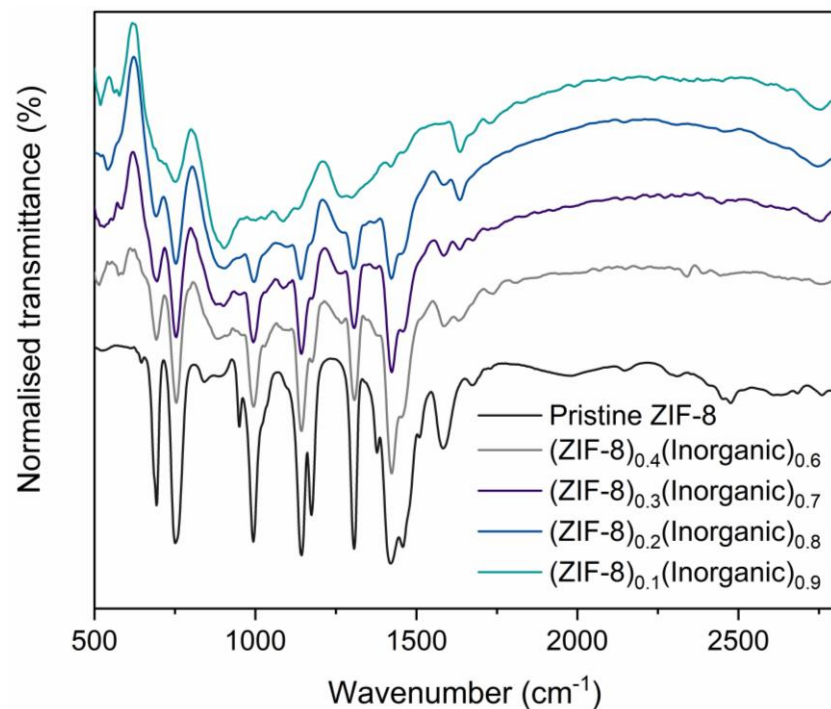


Figure S17. Normalised FTIR spectra of the composites and starting materials.

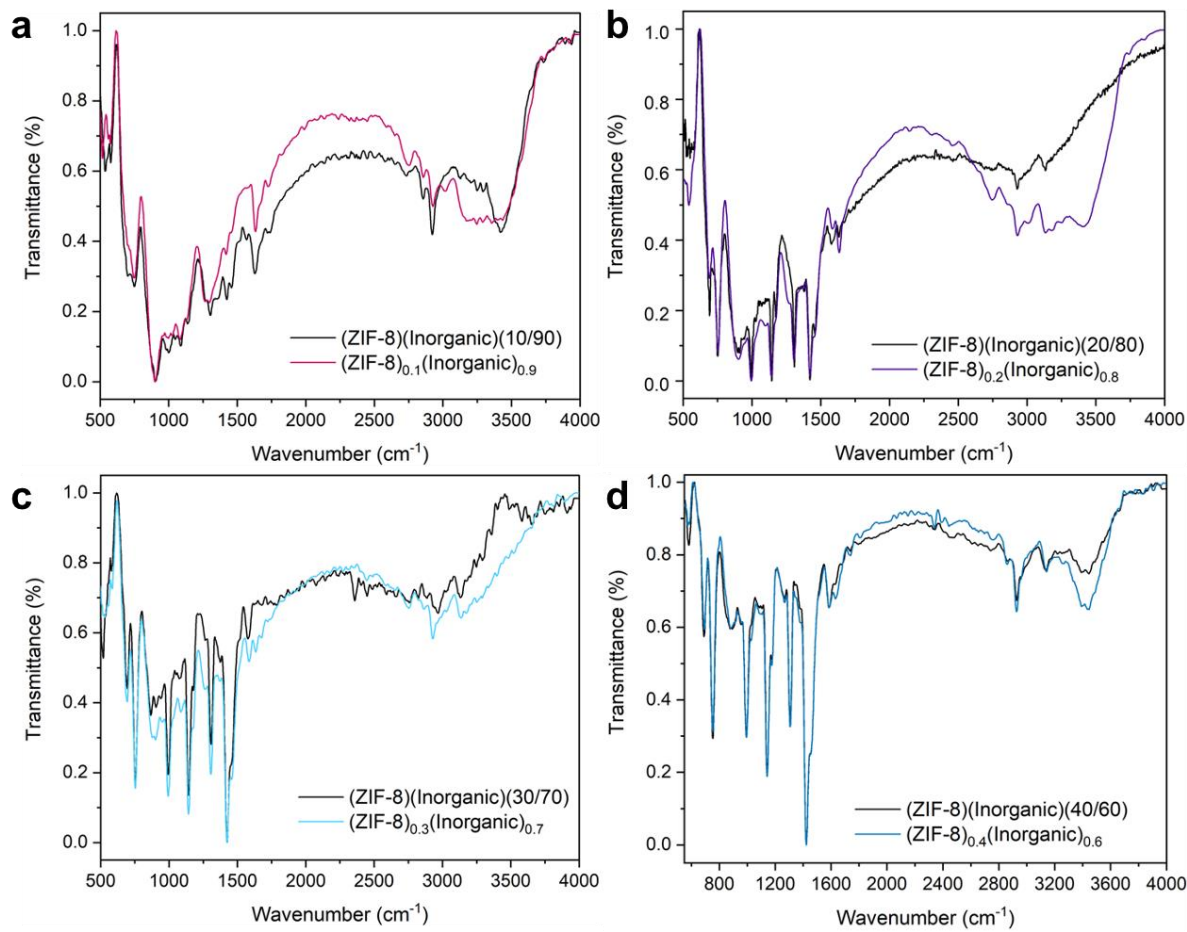


Figure S18. FTIR spectra of the physical mixtures versus the composite post heating for **a.** $(\text{ZIF-8})_{0.1}(\text{Inorganic})_{0.9}$, **b.** $(\text{ZIF-8})_{0.2}(\text{Inorganic})_{0.8}$, **c.** $(\text{ZIF-8})_{0.3}(\text{Inorganic})_{0.7}$ and **d.** $(\text{ZIF-8})_{0.4}(\text{Inorganic})_{0.6}$. $(\text{ZIF-8})(\text{Inorganic})(X/Y)$ denotes the physical mixtures.

4.3 Raman spectroscopy

Raman bands for the ZIF-8 starting material were largely consistent with assignments obtained from the literature.⁵

Table S7. Raman bands of ZIF-8.

Frequency (cm ⁻¹)	Assignment
285	Zn-N stretching
642	Torsion of imidazolate ring
686	Imidazolate (out of plane) ring puckering
837, 953, 1024	C-H out of plane bending
1148	C-N stretching
1182	C-H stretching
1188	C-N stretching

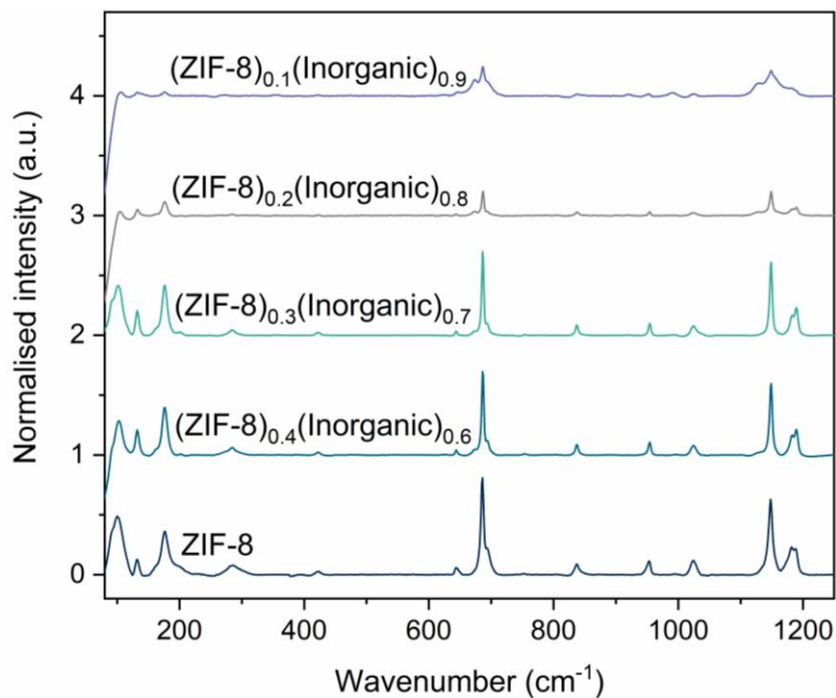


Figure S19. Raman spectra of the composites and pristine ZIF-8 starting material, where intensity has been normalised (0-1) and baseline subtraction has been performed on all samples.

4.4 ^1H NMR spectroscopy

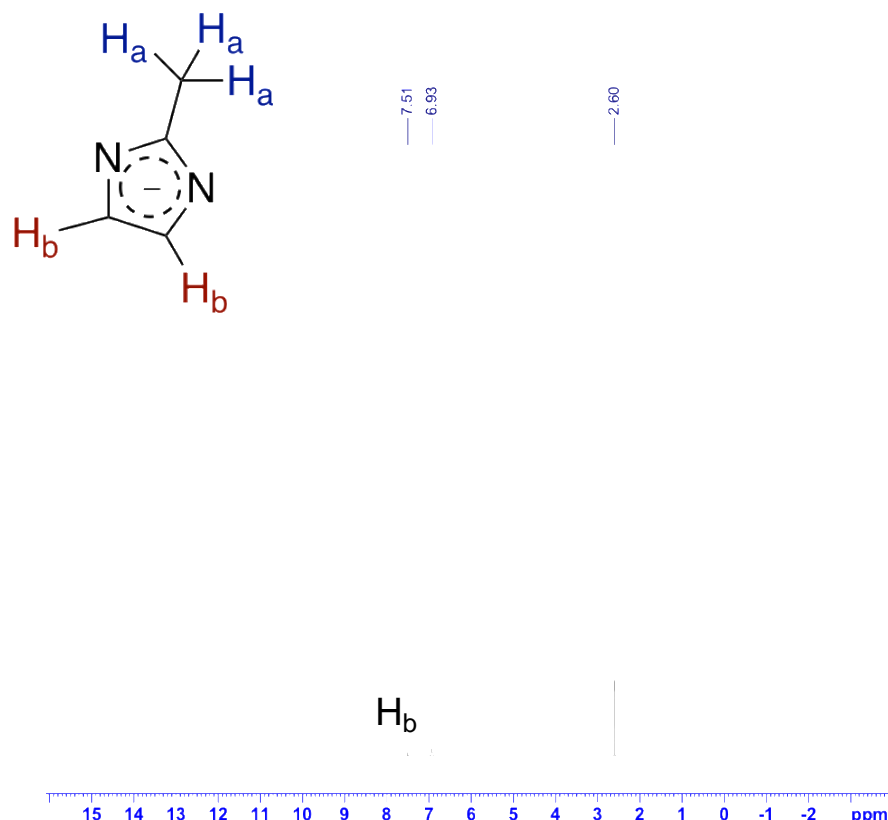


Figure S20. ^1H NMR spectrum of $(\text{ZIF-8})_{0.1}(\text{Inorganic})_{0.9}$ composite. δ_{H} (500 MHz, DCI (35%)/ D_2O : DMSO- d_6 (1:5), TMS) 7.51 (2H, s, H_b), 6.93 (s, $\text{D}_2\text{O}/\text{DCI}$ solvent) 2.60 (m, DMSO- d_6), 0.00 (TMS).

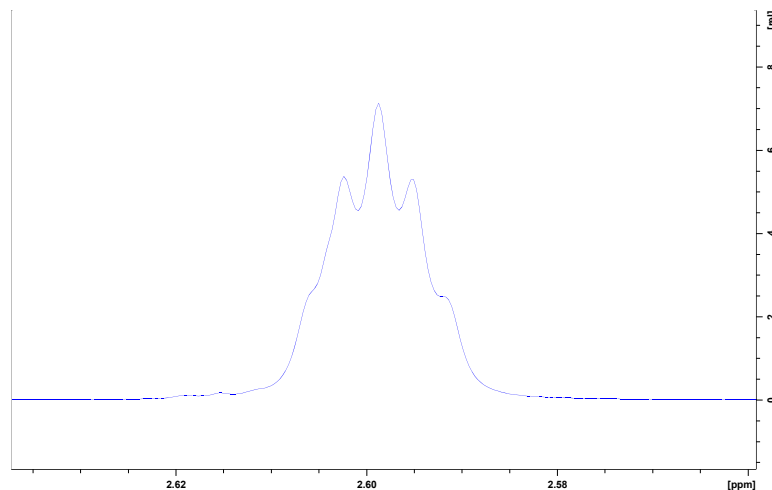


Figure S21. Zoomed in region of ^1H spectrum of $(\text{ZIF-8})_{0.1}(\text{Inorganic})_{0.9}$ composite, showing no H_a environment next to DMSO- d_6 peak.

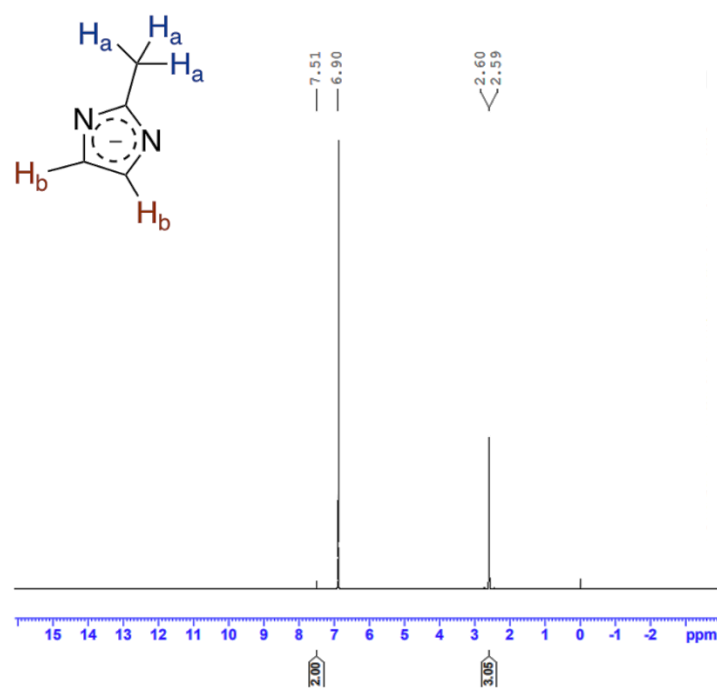


Figure S22. ^1H NMR spectrum of $(\text{ZIF-8})_{0.2}(\text{Inorganic})_{0.8}$ composite. δ_{H} (500 MHz, DCI (35%)/ D_2O : DMSO-d_6 (1:5), TMS) 7.51 (2H, s, H_b), 6.90 (s, $\text{D}_2\text{O}/\text{DCl}$ solvent) 2.6 (3H, s, H_a), 2.59 (m, DMSO-d_6^6), 0.00 (TMS).

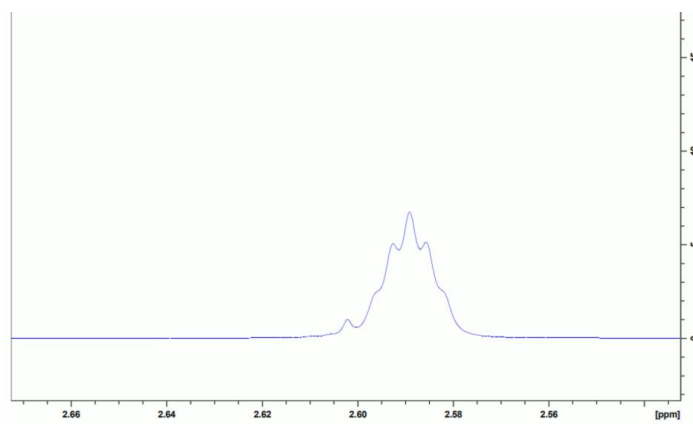


Figure S23. Zoomed in region of ^1H spectrum of the $(\text{ZIF-8})_{0.2}(\text{Inorganic})_{0.8}$ composite, showing H_a environment next to the DMSO-d_6 peak.

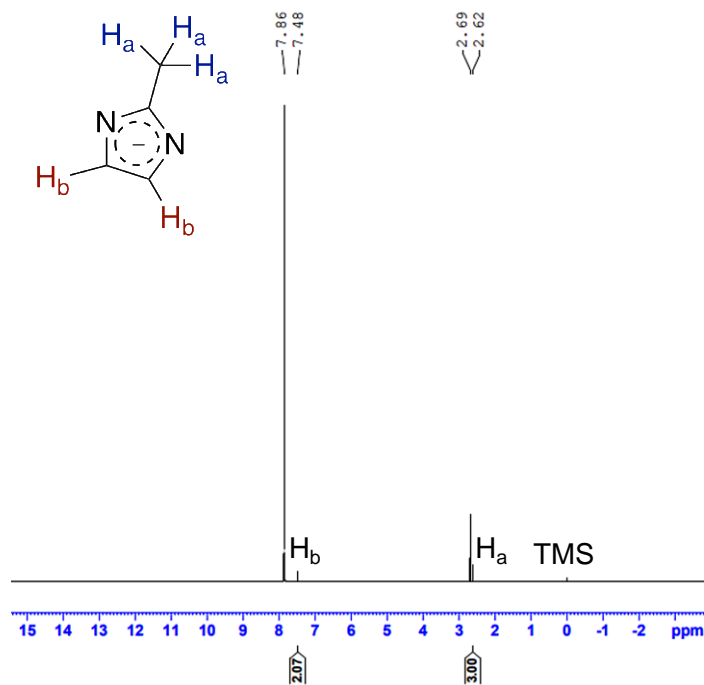


Figure S24. ¹H NMR spectrum of (ZIF-8)_{0.3}(Inorganic)_{0.7} composite. δ_{H} (500 MHz, DCI (35%)/D₂O: DMSO-d₆ (1:5), TMS) 7.86 (s, D₂O/DCI solvent), 7.48 (2H, s, H_b), 2.69 (m, DMSO-d₆), 2.62 (3H, s, H_a), 0.00 (TMS).

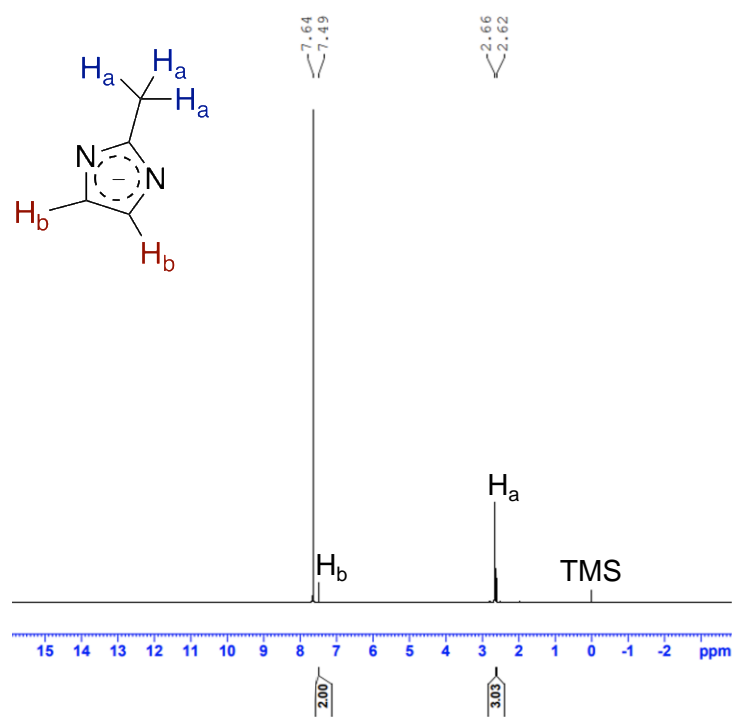


Figure S25. ¹H NMR spectrum of (ZIF-8)_{0.4}(Inorganic)_{0.6} composite. δ_{H} (500 MHz, DCI (35%)/D₂O: DMSO-d₆ (1:5), TMS) 7.64 (s, D₂O/DCI solvent), 7.49 (2H, s, H_b), 2.66 (m, DMSO-d₆), 2.62 (3H, s, H_a), 0.00 (TMS).

4.5 SEM-EDS

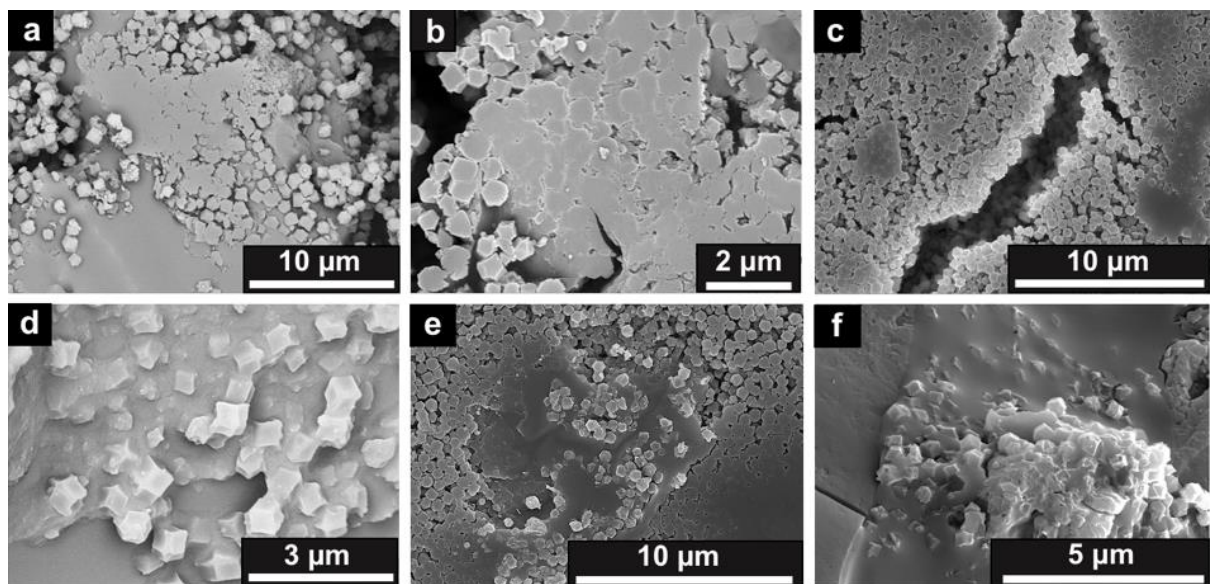


Figure S26. SEM images of the $(\text{ZIF-8})_{0.1}(\text{Inorganic})_{0.9}$ composite (a, d), $(\text{ZIF-8})_{0.2}(\text{Inorganic})_{0.8}$ composite (b, e) and $(\text{ZIF-8})_{0.4}(\text{Inorganic})_{0.6}$ composite (c, f).

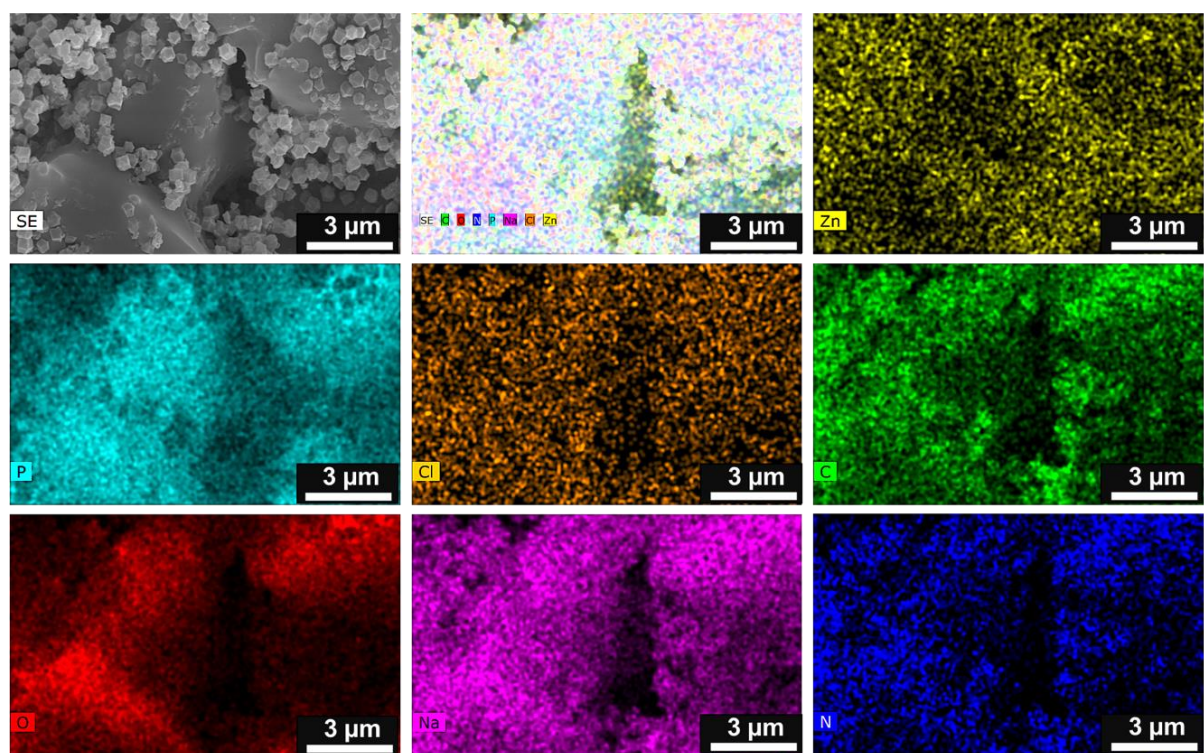


Figure S27. SEM-EDX mapping of the $(\text{ZIF-8})_{0.1}(\text{Inorganic})_{0.9}$ composite using an accelerating voltage of 15 kV.

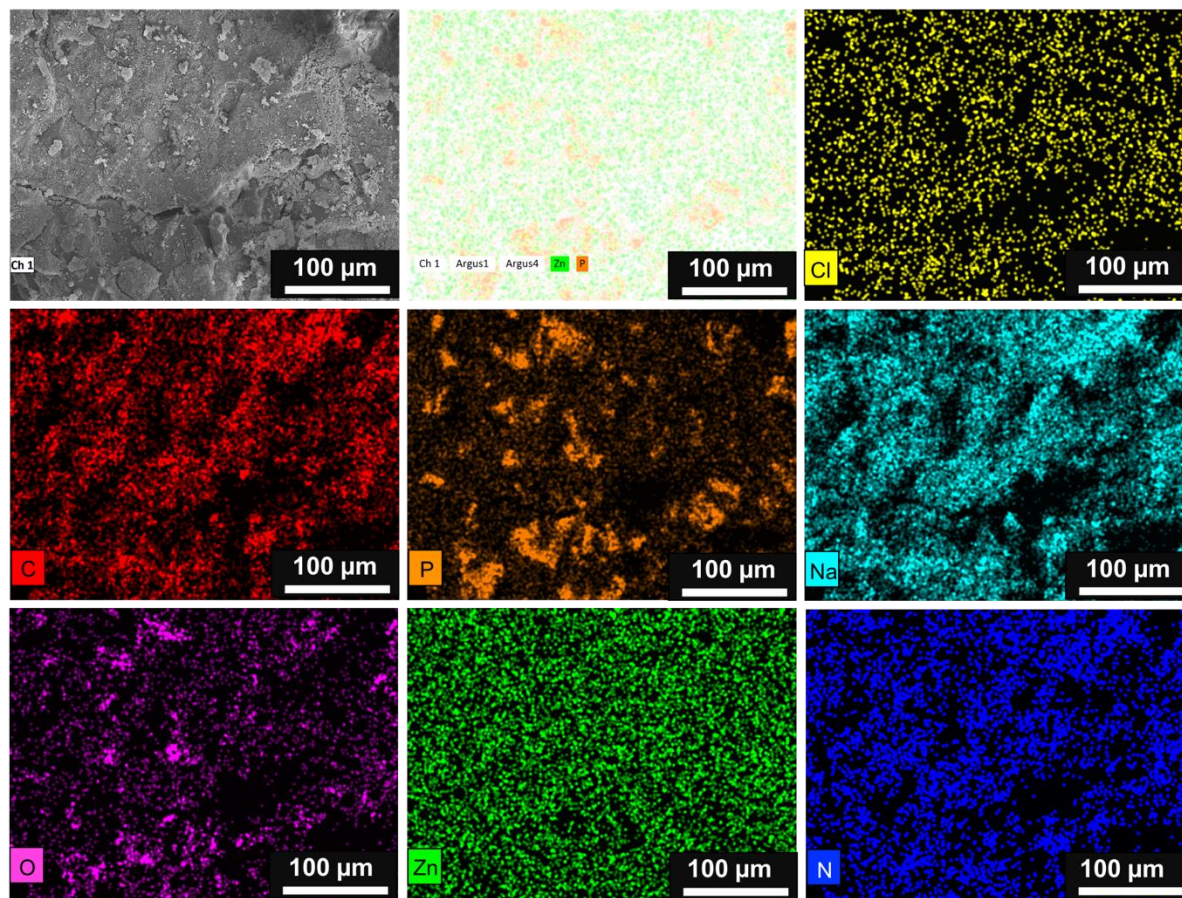


Figure S28. SEM-EDX mapping of the $(\text{ZIF-8})_{0.2}(\text{Inorganic})_{0.8}$ composite using an accelerating voltage of 15 kV.

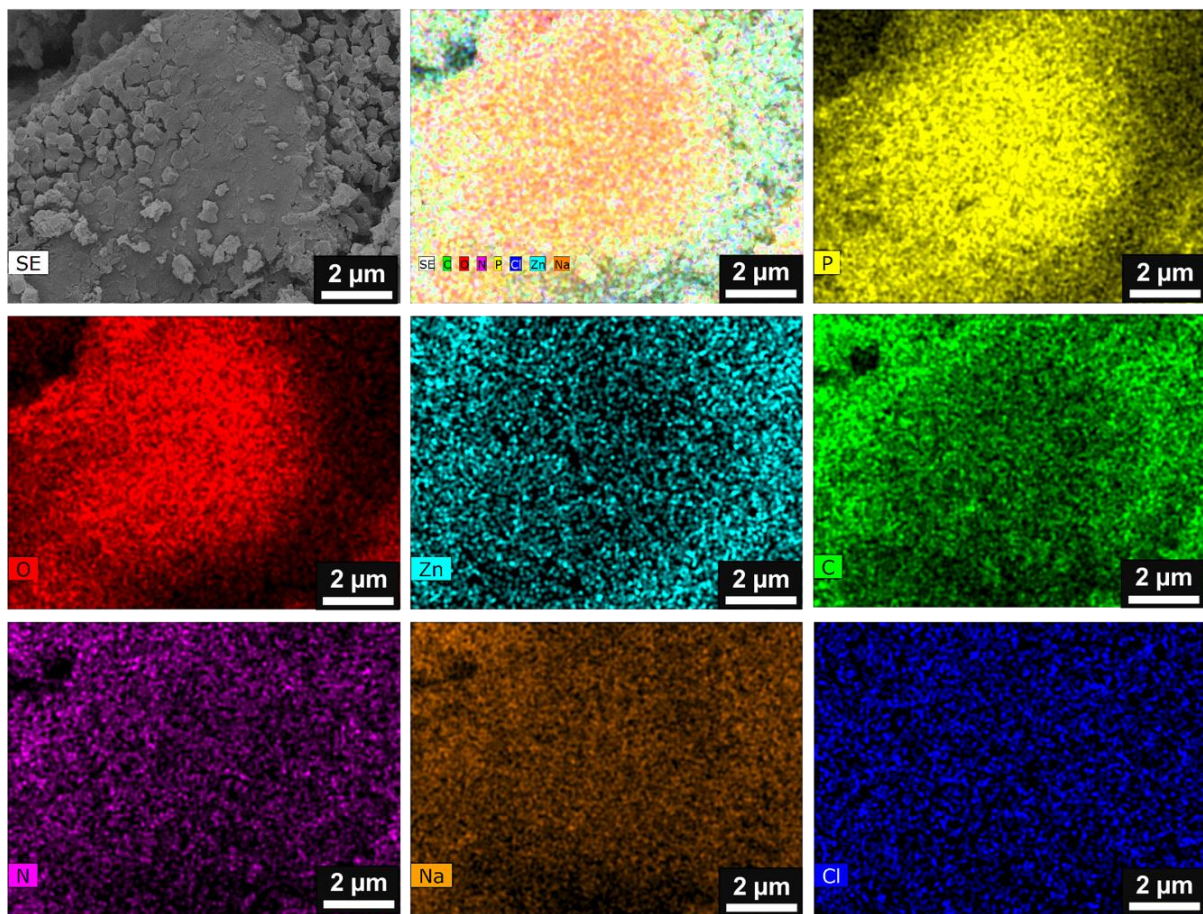


Figure S29. SEM-EDX mapping of the $(\text{ZIF-8})_{0.3}(\text{Inorganic})_{0.7}$ composite using an accelerating voltage of 15 kV.

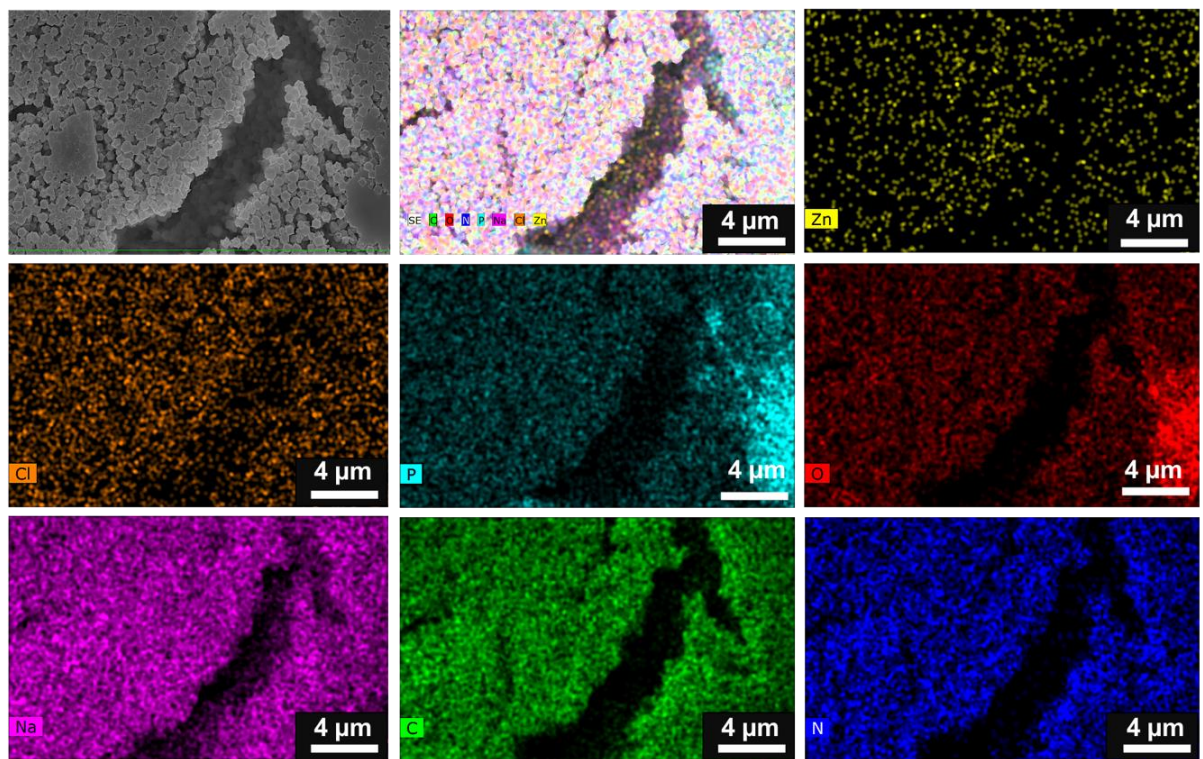


Figure S30. SEM-EDX mapping of the $(\text{ZIF-8})_{0.4}(\text{Inorganic})_{0.6}$ composite using an accelerating voltage of 15 kV.

4.6 Thermal analysis

Initial mass losses observed likely correspond to water loss because the inorganic glass is hygroscopic.

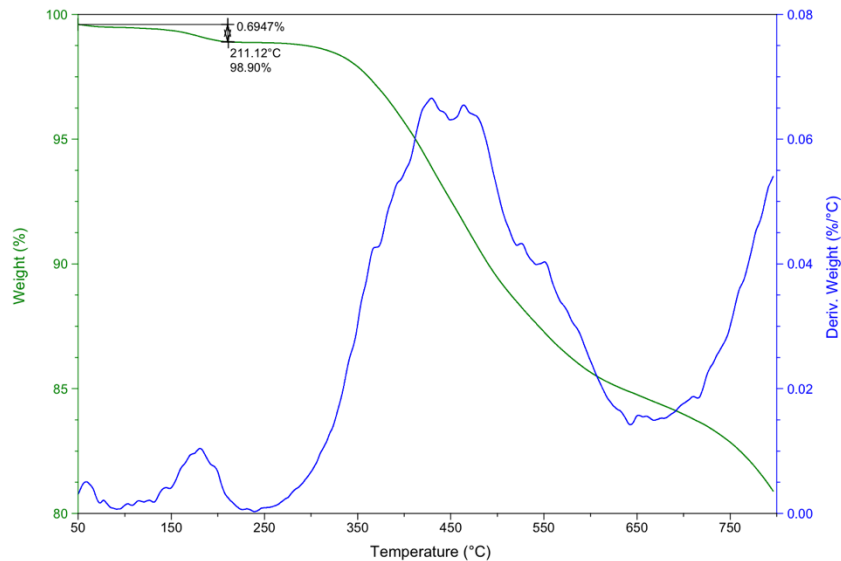


Figure S31. TGA trace of (ZIF-8)(Inorganic)(10/90) mixture.

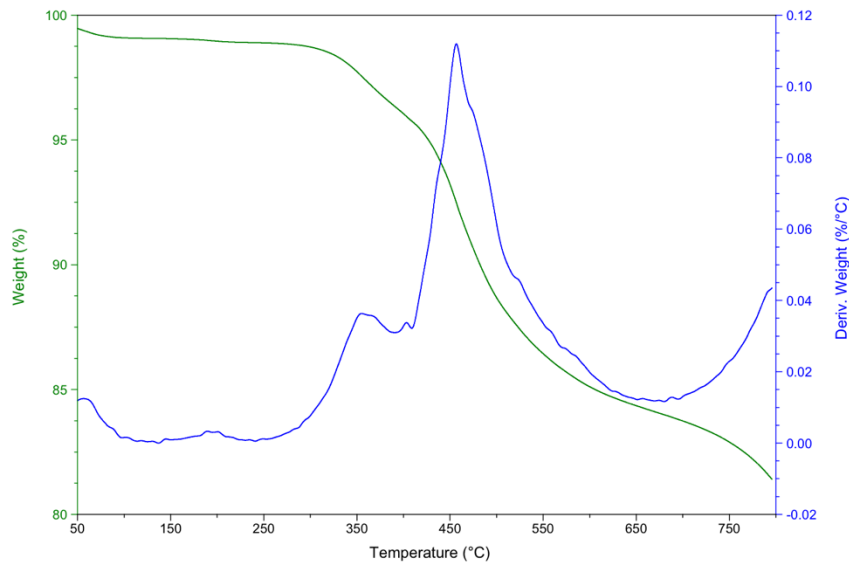


Figure S32. TGA trace of (ZIF-8)(Inorganic)(20/80) mixture.

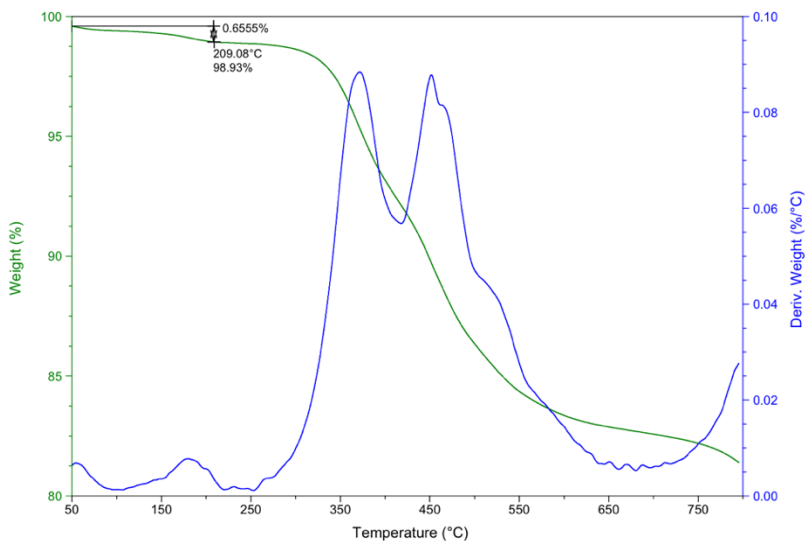


Figure S33. TGA trace of (ZIF-8)(Inorganic)(30/70) mixture.

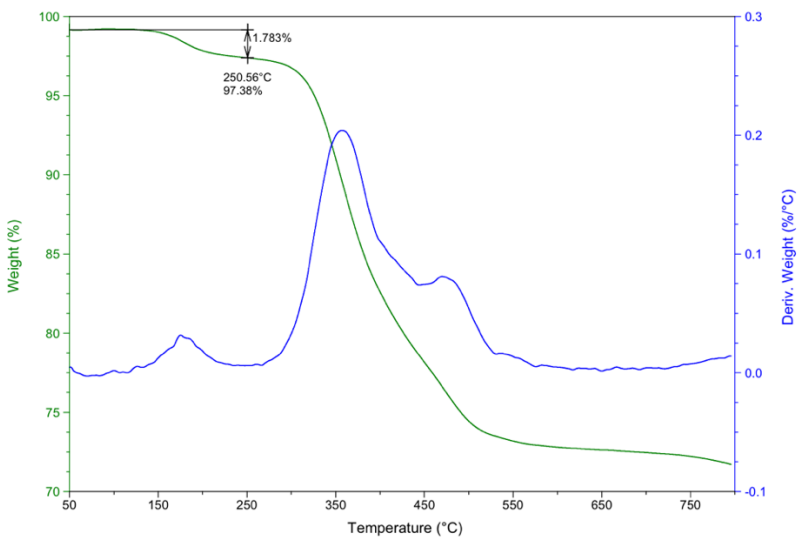


Figure S34. TGA trace of (ZIF-8)(Inorganic)(40/60) mixture.

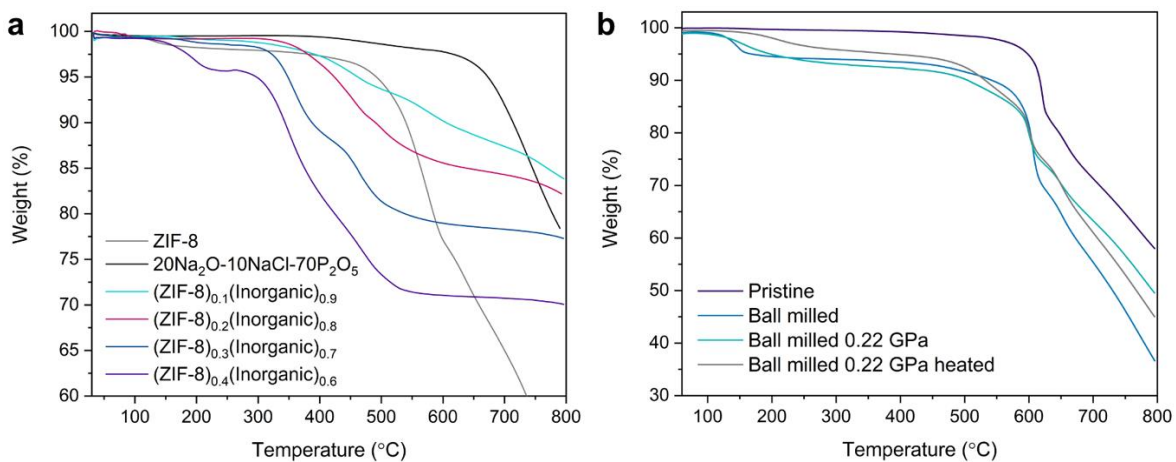


Figure S35. TGA curves of **a.** The composites and starting materials and **b.** ZIF-8 controls: pristine, ball-milled (20 Hz, 5 min), pelletised and ball-milled and ball-milled, pelletised and heat treated ZIF-8 (20 Hz, 5 min, 0.22 GPa, 200 °C for 30 minutes).

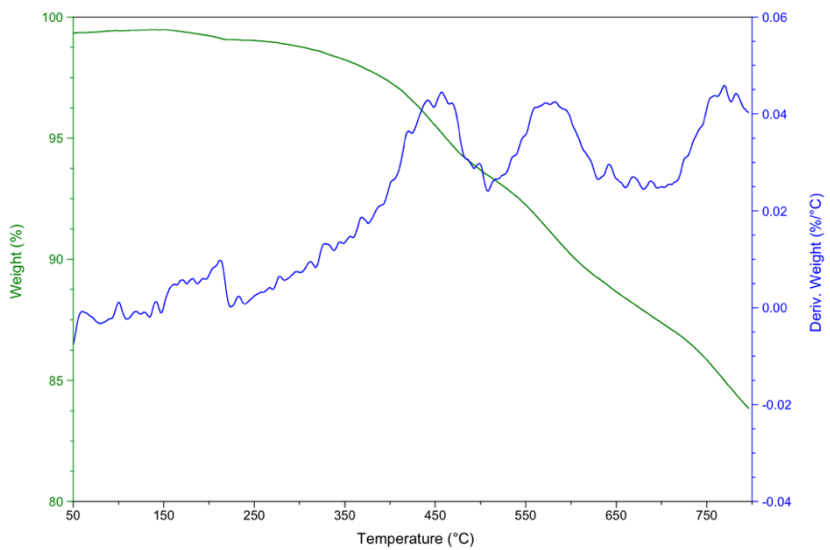


Figure S36. TGA trace of $(\text{ZIF-8})_{0.1}(\text{Inorganic})_{0.9}$ composite.

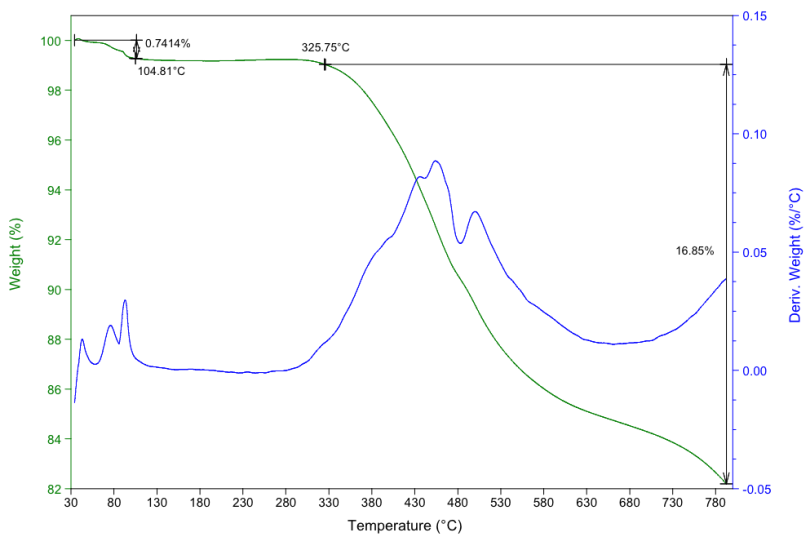


Figure S37. TGA trace of $(\text{ZIF-8})_{0.2}(\text{Inorganic})_{0.8}$ composite.

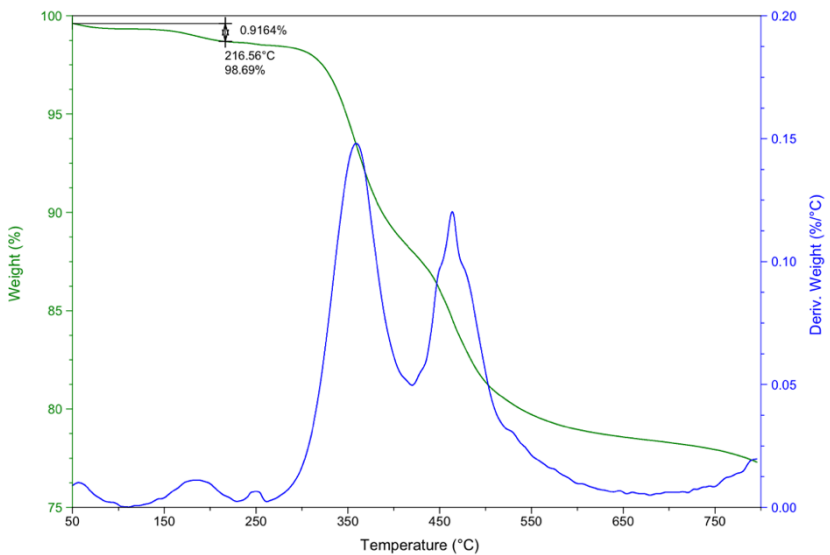


Figure S38. TGA trace of $(\text{ZIF-8})_{0.3}(\text{Inorganic})_{0.7}$ composite.

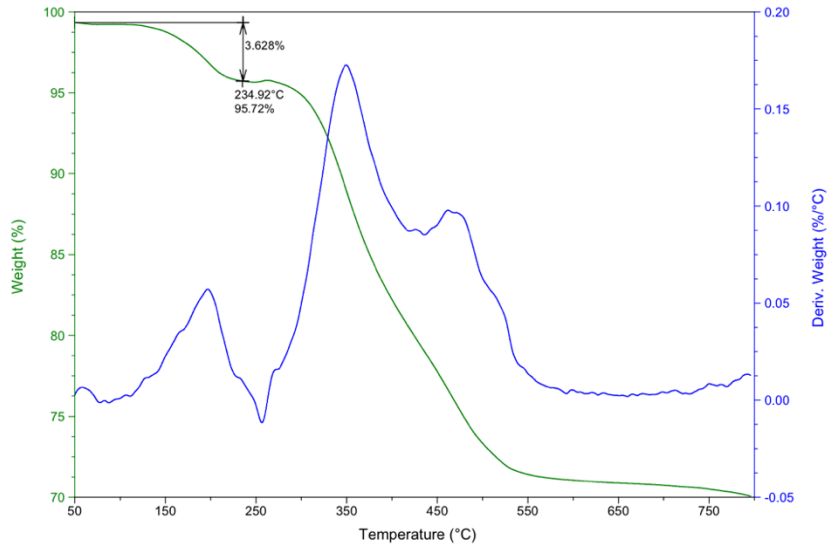


Figure S39. TGA trace of $(\text{ZIF-8})_{0.4}(\text{Inorganic})_{0.6}$ composite.

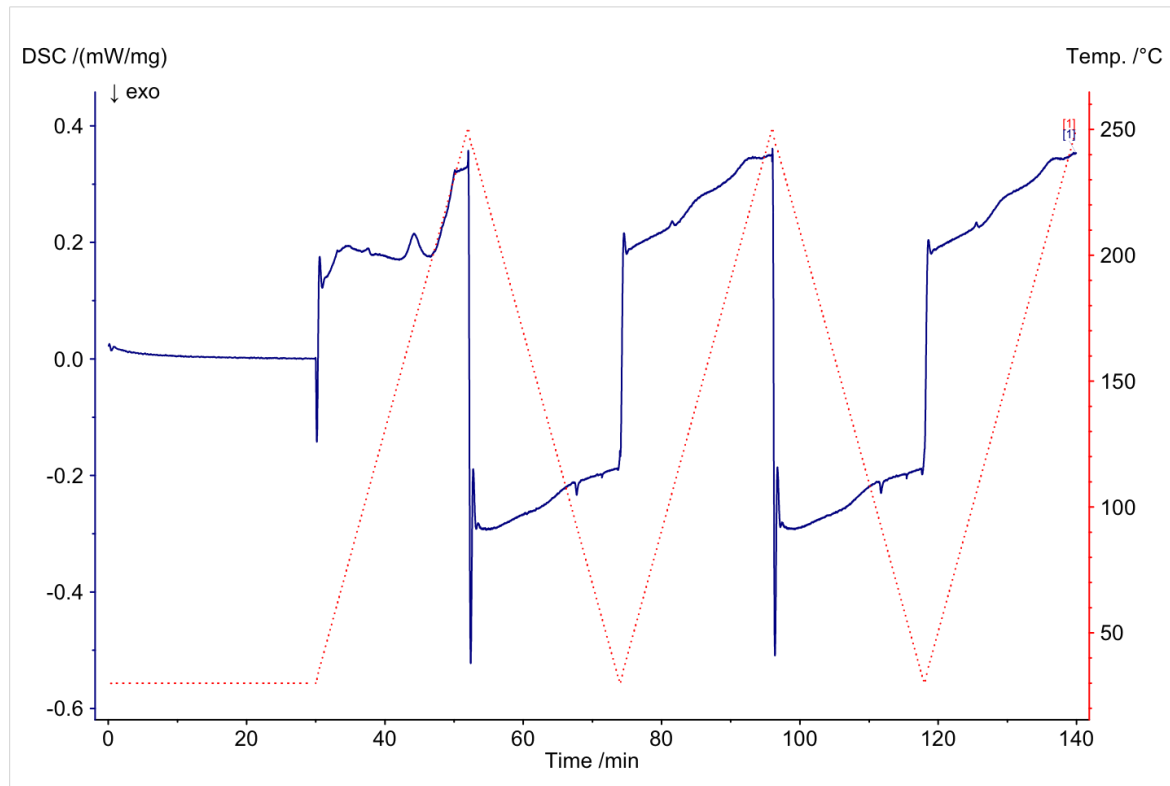


Figure S40. Full DSC up and down scans of the $(\text{ZIF-8})_{0.1}(\text{Inorganic})_{0.9}$ composite using a heating rate of $10 \text{ }^{\circ}\text{C} \text{ min}^{-1}$ and a heating range of $30\text{--}250 \text{ }^{\circ}\text{C}$.

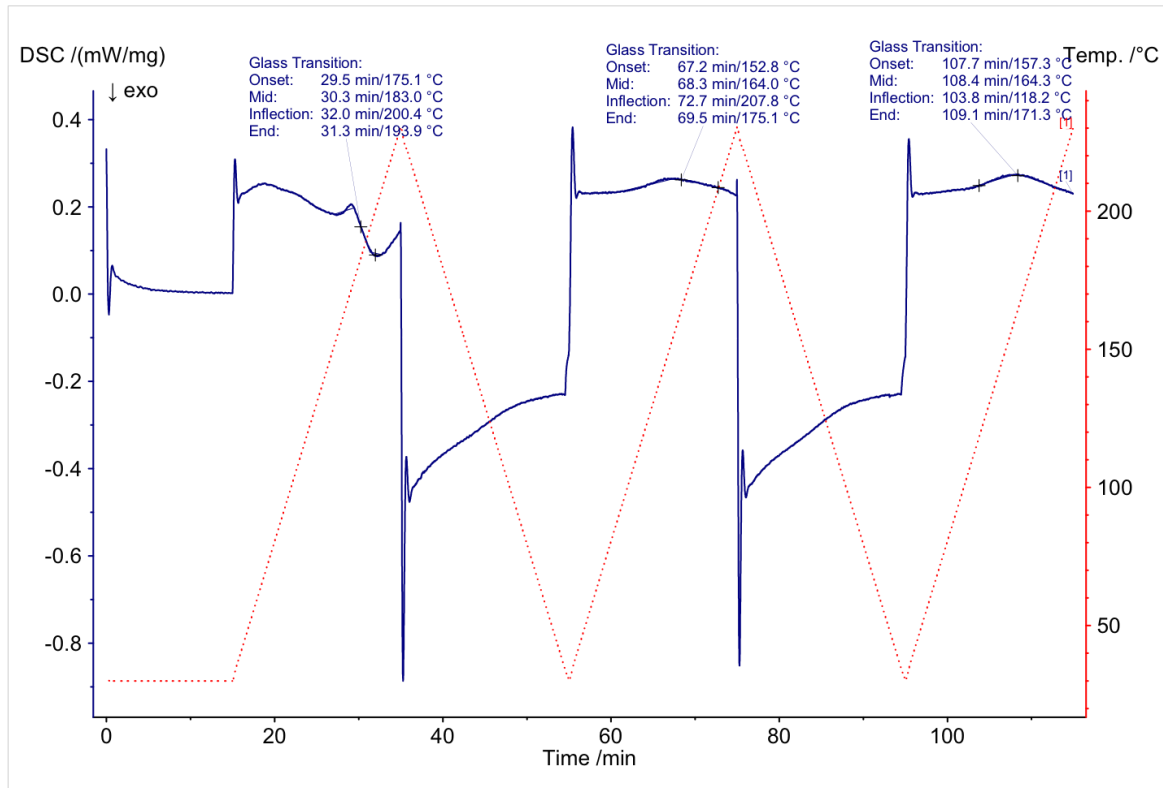


Figure S41. Full DSC up and down scans of the $(\text{ZIF-8})_{0.2}(\text{Inorganic})_{0.8}$ composite, using a heating rate of $10 \text{ }^{\circ}\text{C min}^{-1}$ and a heating range of $30\text{--}230 \text{ }^{\circ}\text{C}$.

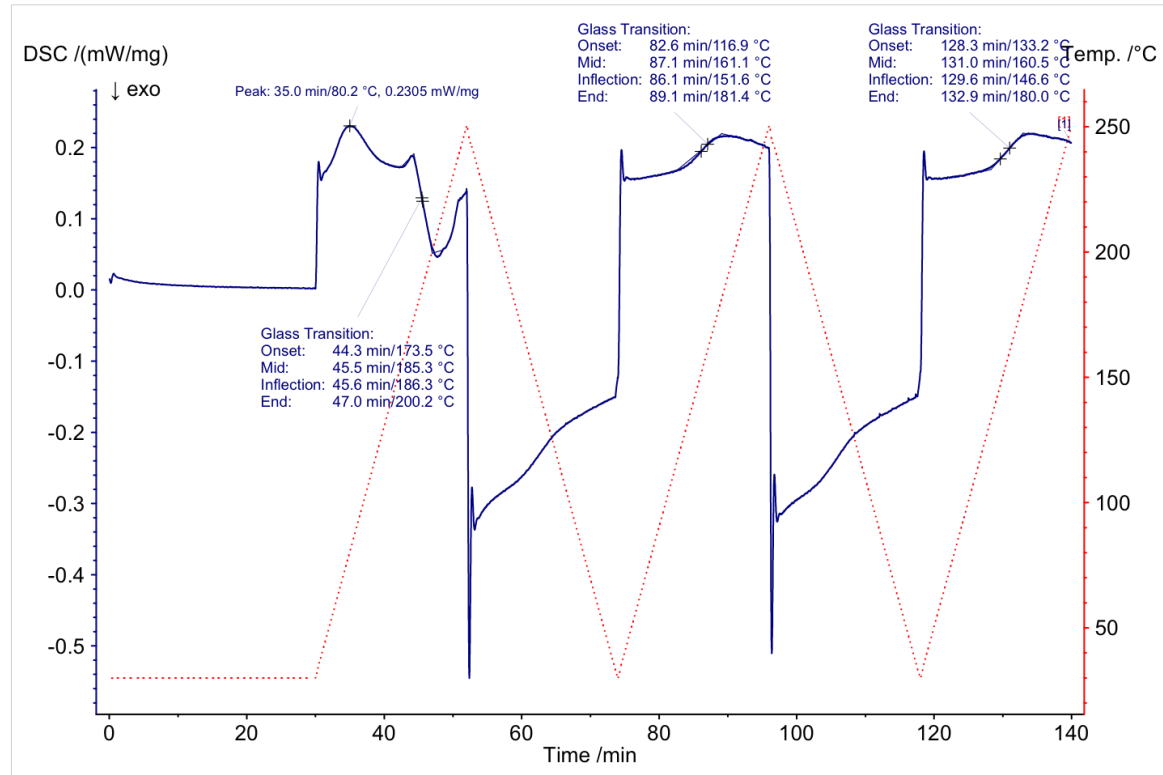


Figure S42. Full DSC up and down scans of the $(\text{ZIF-8})_{0.3}(\text{Inorganic})_{0.7}$ composite, using a heating rate of $10 \text{ }^{\circ}\text{C min}^{-1}$ and a heating range of $30\text{--}250 \text{ }^{\circ}\text{C}$.

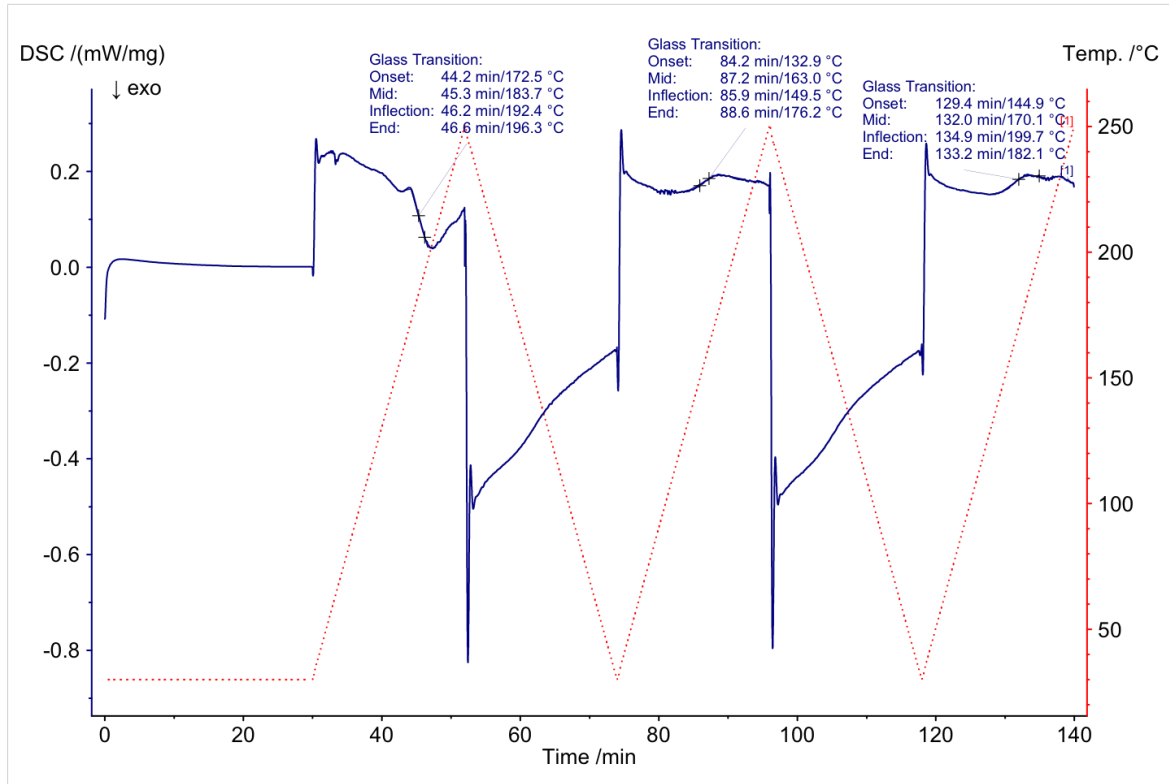


Figure S43. Full DSC up and down scans of the $(\text{ZIF-8})_{0.4}(\text{Inorganic})_{0.6}$ composite, using a heating rate of $10 \text{ }^{\circ}\text{C} \text{ min}^{-1}$ and a heating range of $30\text{--}250 \text{ }^{\circ}\text{C}$.

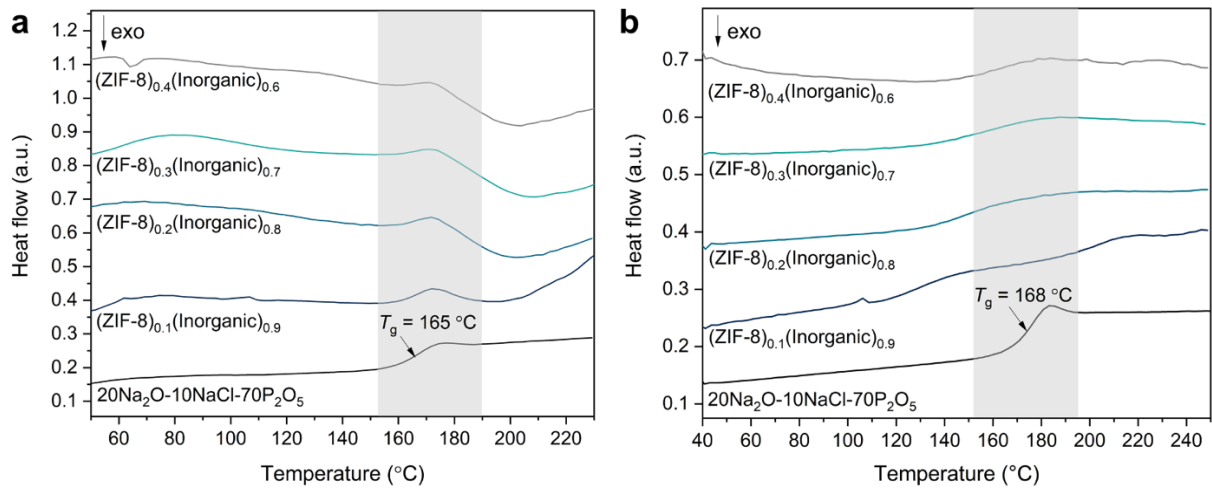


Figure S44. **a.** 1st DSC upscan of the composites and inorganic glass and **b.** 3rd DSC upscan of the composites and inorganic glass, showing the reproducibility of the features identified in the 2nd DSC upscan (main text). Shaded regions denote the glass transition range of the inorganic glass.

4.7 PDF analysis

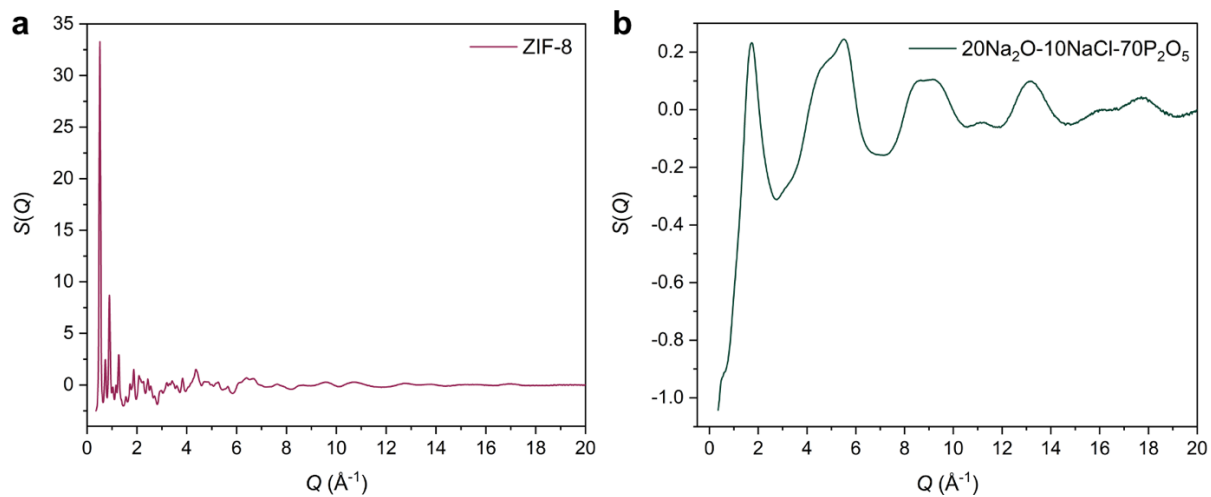


Figure S45. X-ray total scattering structure factor, $S(Q)$, of pristine **a.** ZIF-8 and **b.** 20Na₂O-10NaCl-70P₂O₅.

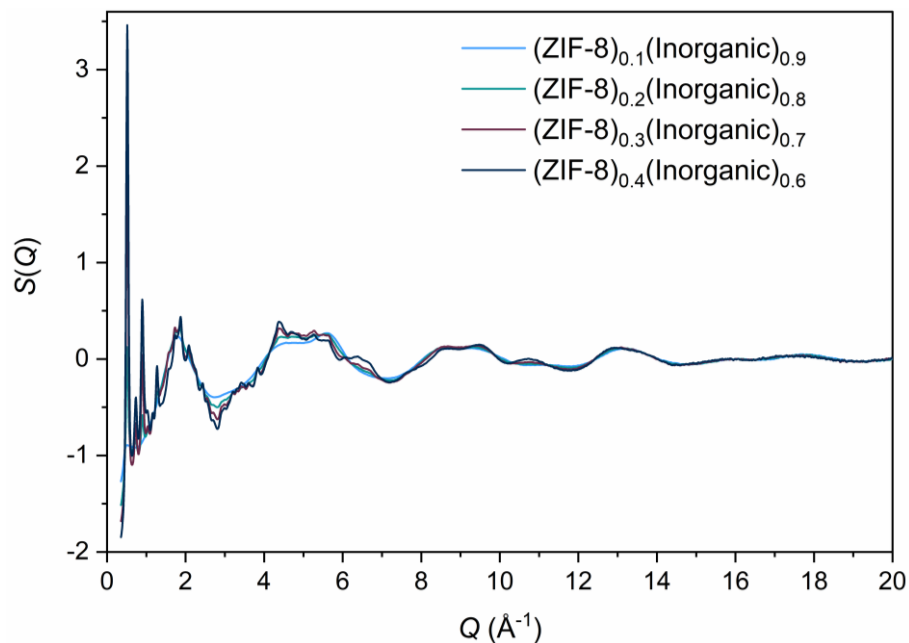


Figure S46. X-ray total scattering structure factor, $S(Q)$, data of the four composites.

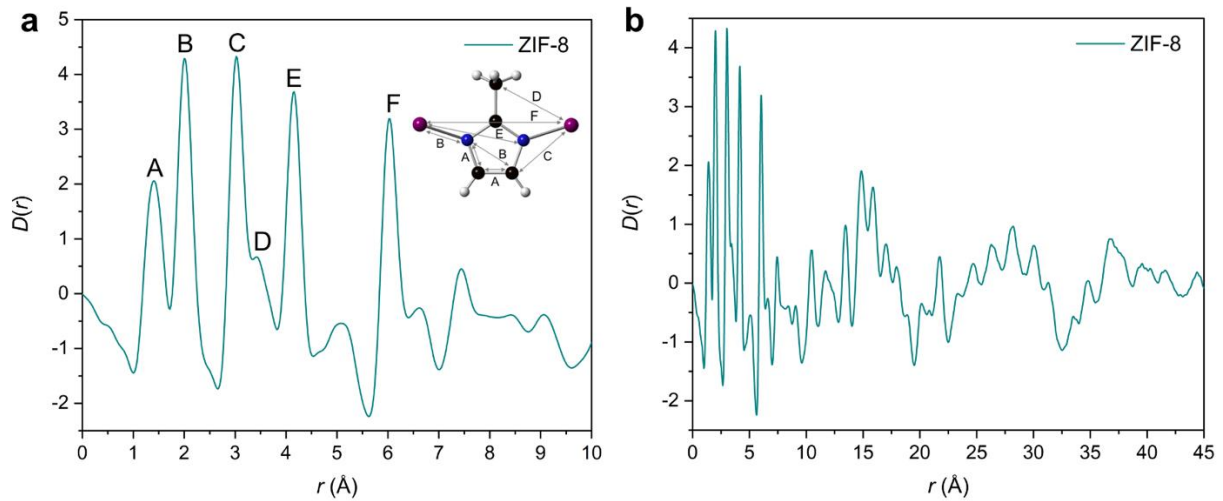


Figure S47. X-ray pair distribution function $D(r)$ of pristine ZIF-8 at **a.** $r = 0\text{-}10 \text{\AA}$ (local order) and **b.** $r = 0\text{-}45 \text{\AA}$.

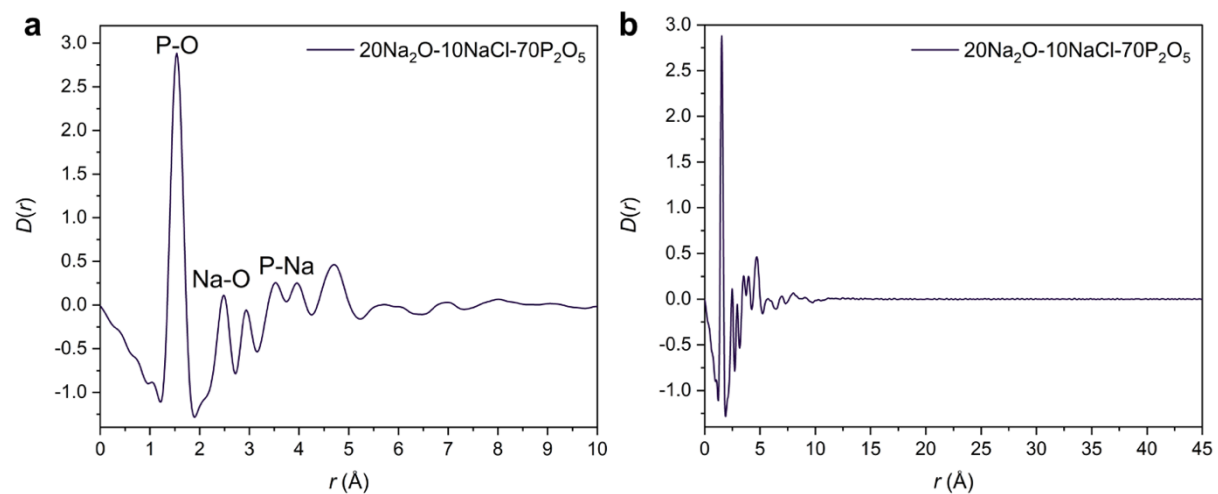


Figure S48. X-ray pair distribution function $D(r)$ of pristine 20Na₂O-10NaCl-70P₂O₅ **a.** $r = 0\text{-}10 \text{\AA}$ (local order) and **b.** $r = 0\text{-}45 \text{\AA}$, showing a lack of long-range order.

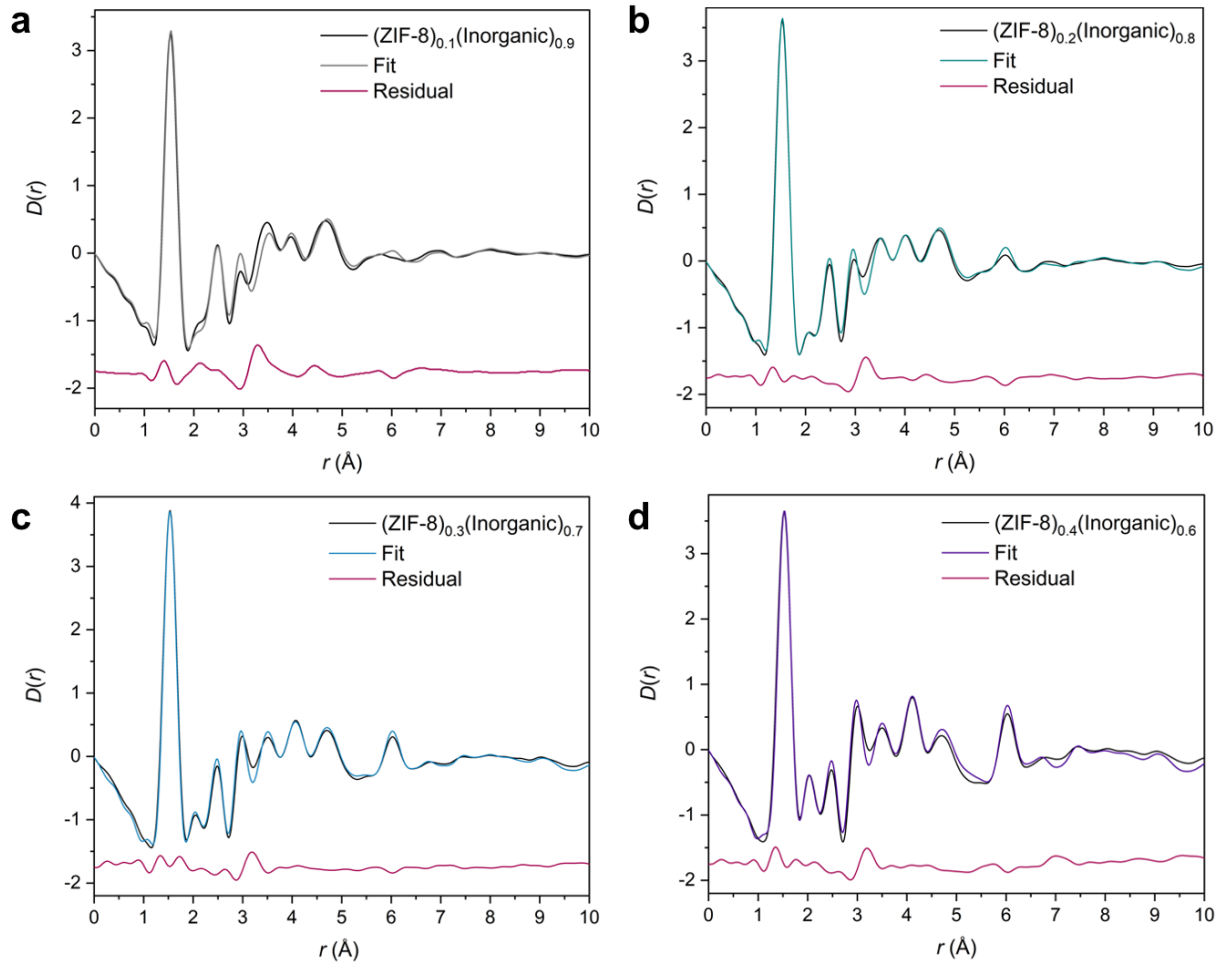


Figure S49. X-ray pair distribution function $D(r)$ and MLR fit of **a.** $(\text{ZIF-8})_{0.1}(\text{Inorganic})_{0.9}$ **b.** $(\text{ZIF-8})_{0.2}(\text{Inorganic})_{0.8}$ **c.** $(\text{ZIF-8})_{0.3}(\text{Inorganic})_{0.7}$ and **d.** $(\text{ZIF-8})_{0.4}(\text{Inorganic})_{0.6}$.

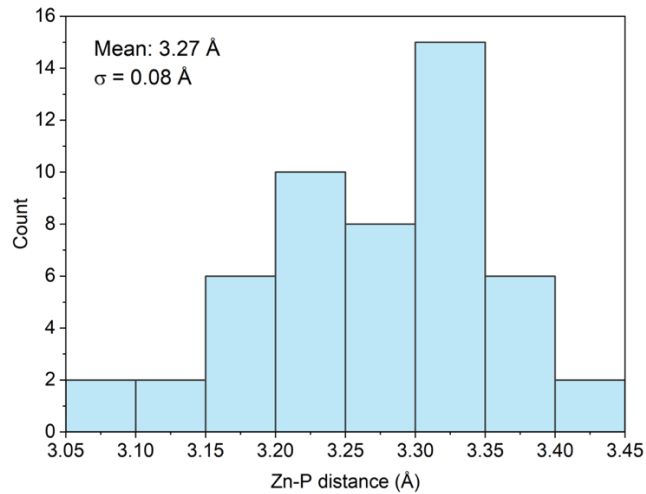


Figure S50. Average Zn-P distance via a bridging oxygen atom from three crystalline zinc phosphate CIFs, CCDC numbers 1007095 ($\text{Zn}(\text{PO}_3)_2$), 2310787 ($\alpha\text{-Zn}_2\text{P}_2\text{O}_7$) and 2310789 ($\beta\text{-Zn}_2\text{P}_2\text{O}_7$).⁶

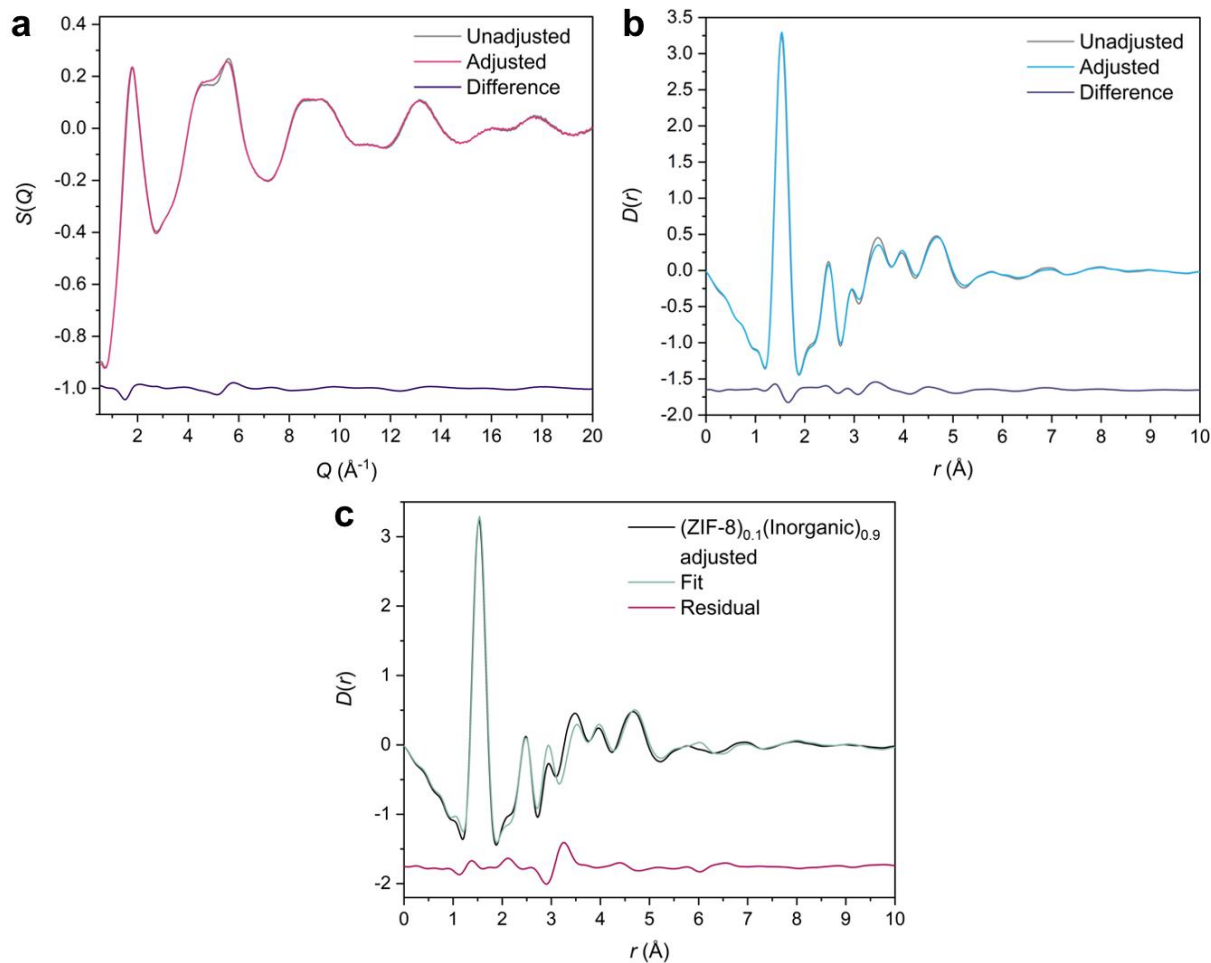


Figure S51. **a.** Comparison of the $S(Q)$ plots of the $(\text{ZIF-8})_{0.1}(\text{Inorganic})_{0.9}$, **b.** Comparison of $(\text{ZIF-8})_{0.1}(\text{Inorganic})_{0.9} D(r)$ before and after data adjustment, indicating a negative peak at $r = 1.66 \text{ \AA}$ in the difference curve and **c.** MLR fit of the *adjusted* $(\text{ZIF-8})_{0.1}(\text{Inorganic})_{0.9}$.

Table S8. Multiple linear regression parameters obtained from the fitting.

Sample	C_1	C_2	Adjusted R^2	Reduced χ^2
10% ZIF-8 (unadjusted)	1.13 ± 0.007	0.02 ± 0.003	0.979	0.008
10% ZIF-8 (adjusted)	1.14 ± 0.006	0.02 ± 0.001	0.987	0.005
20% ZIF-8	1.23 ± 0.004	0.07 ± 0.002	0.989	0.004
30% ZIF-8	1.28 ± 0.004	0.13 ± 0.001	0.991	0.004
40% ZIF-8	1.17 ± 0.007	0.22 ± 0.003	0.983	0.008

4.8 CO₂ adsorption

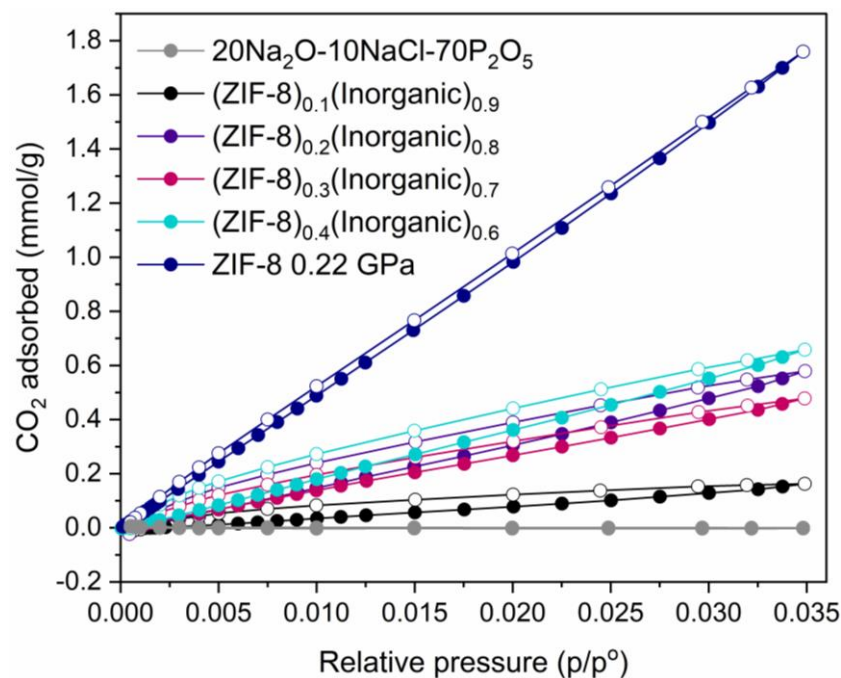


Figure S52. CO₂ adsorption isotherms of the 10-40 ZIF-8 wt% composites and their parent materials.

Table S9. Maximum CO₂ uptakes values of all samples at a relative pressure of 0.035.

Material	Quantity adsorbed (mmol g ⁻¹)
20Na ₂ O-10NaCl-70P ₂ O ₅	0.056
(ZIF-8) _{0.1} (Inorganic) _{0.9}	0.163
(ZIF-8) _{0.2} (Inorganic) _{0.8}	0.478
(ZIF-8) _{0.3} (Inorganic) _{0.7}	0.579
(ZIF-8) _{0.4} (Inorganic) _{0.6}	0.658
Pelletised ZIF-8 (0.22 GPa)	1.76

4.9 Air stability

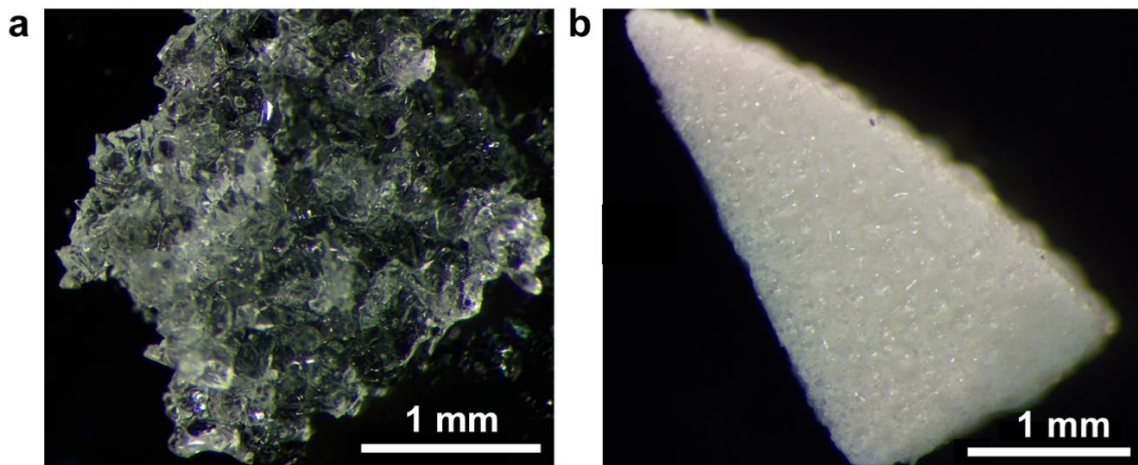


Figure S53. Optical images of **a.** Pristine inorganic glass after air exposure and **b.** Surface of a section of the $(\text{ZIF-8})_{0.4}(\text{Inorganic})_{0.6}$ composite after air exposure. The pellet's form remains intact, but water has been absorbed onto the surface.

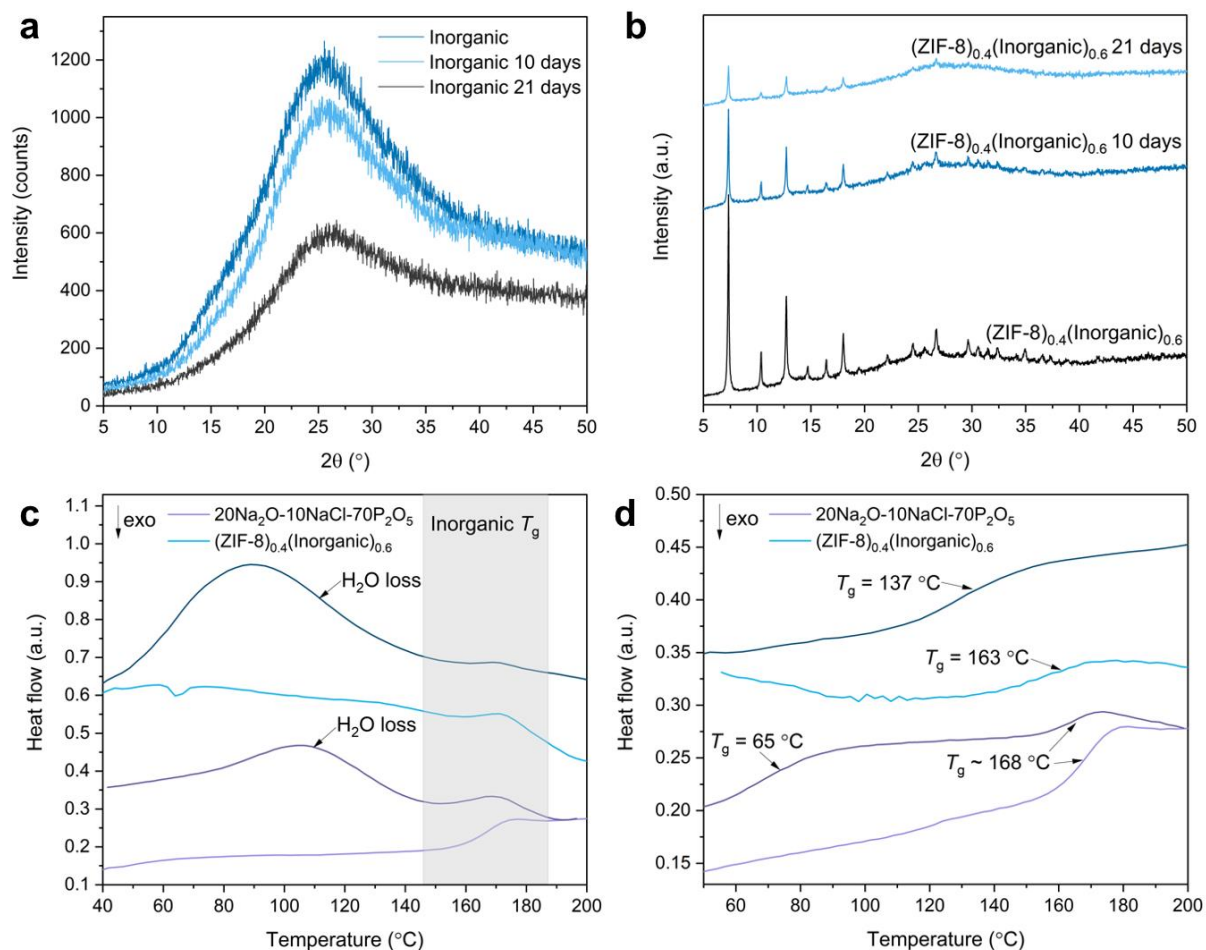


Figure S54. **a.** PXRD of the pristine inorganic glass after air exposure, **b.** PXRD of the $(\text{ZIF-8})_{0.4}(\text{Inorganic})_{0.6}$ composite after air exposure, **c.** 1st and **d.** 2nd DSC upscans of the inorganic glass and $(\text{ZIF-8})_{0.4}(\text{Inorganic})_{0.6}$ before and after three weeks air exposure. Lighter curves correspond to the samples prior to air exposure, darker curves correspond to the samples post air exposure.

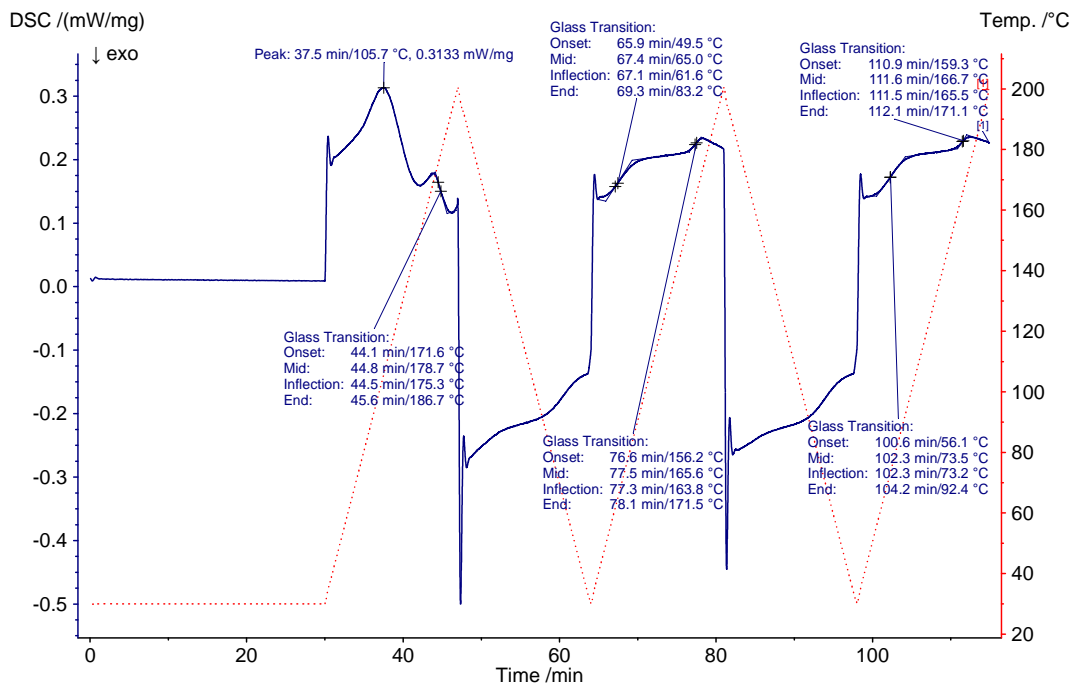


Figure S55. Full DSC up and down scans of the pristine inorganic glass after three weeks air exposure, using a heating range of 30–200 °C and a heating rate of 10 °C min⁻¹.

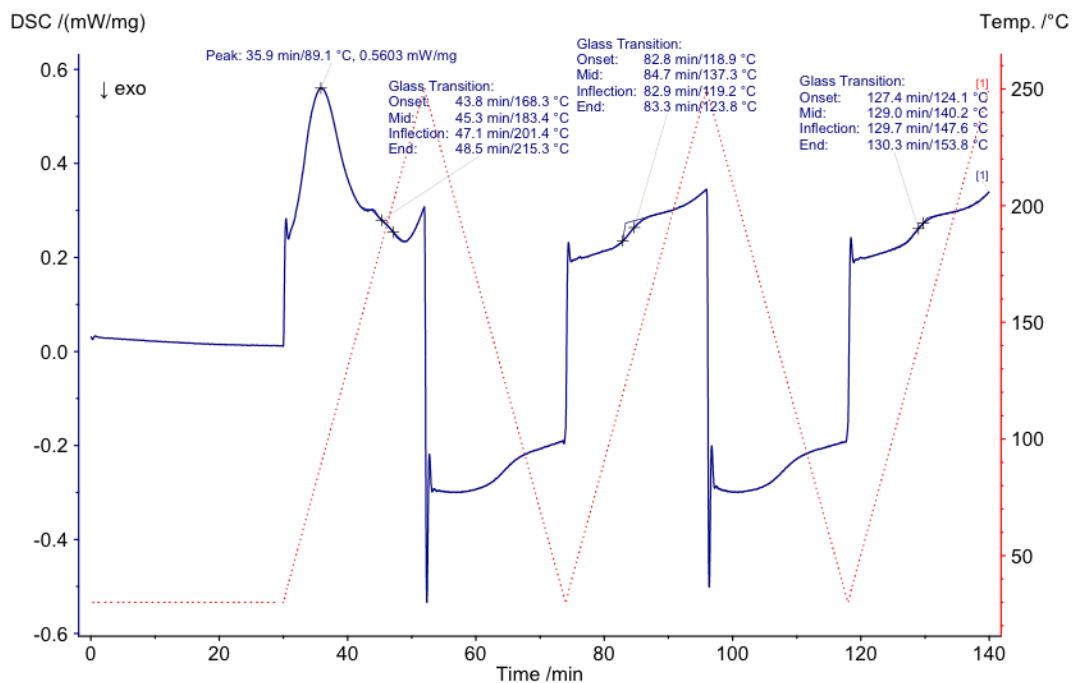


Figure S56. Full DSC scan of pristine (ZIF-8)_{0.4}(Inorganic)_{0.6} composite after three weeks air exposure, using a heating range of 30–250 °C and a heating rate of 10 °C min⁻¹.

4.10 Maximum ZIF-8 loading

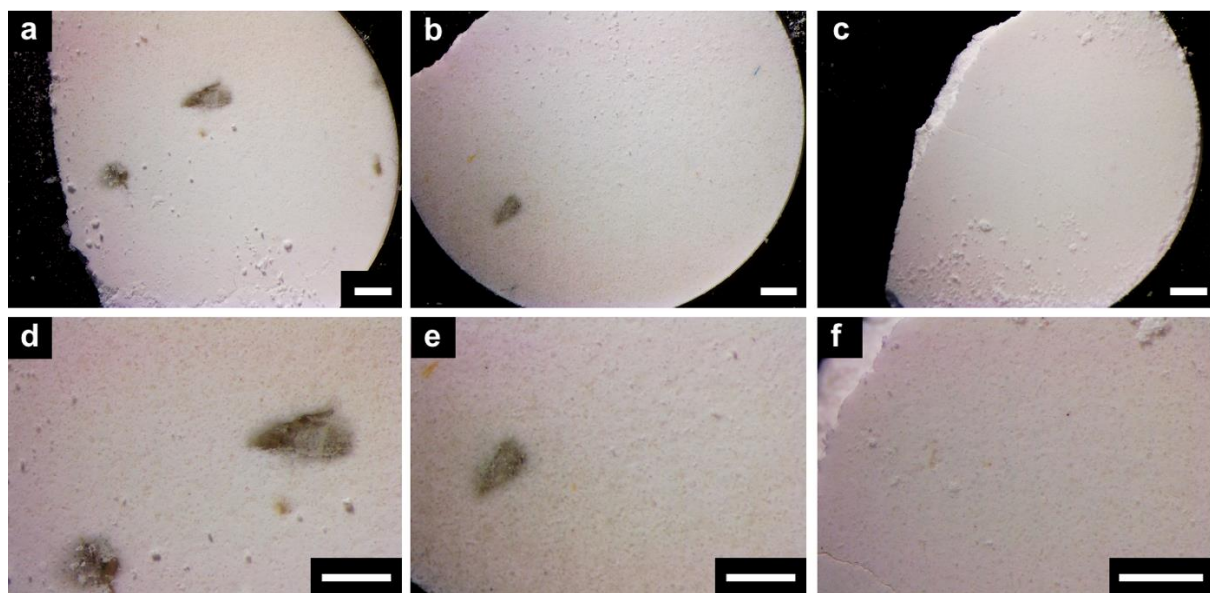


Figure S57. Optical images of the $(\text{ZIF-8})_{0.5}(\text{Inorganic})_{0.5}$ (a, d), $(\text{ZIF-8})_{0.6}(\text{Inorganic})_{0.4}$ (b, e) and $(\text{ZIF-8})_{0.7}(\text{Inorganic})_{0.3}$ (c, f) composites post heating. Scale bar is 1 mm for all images.

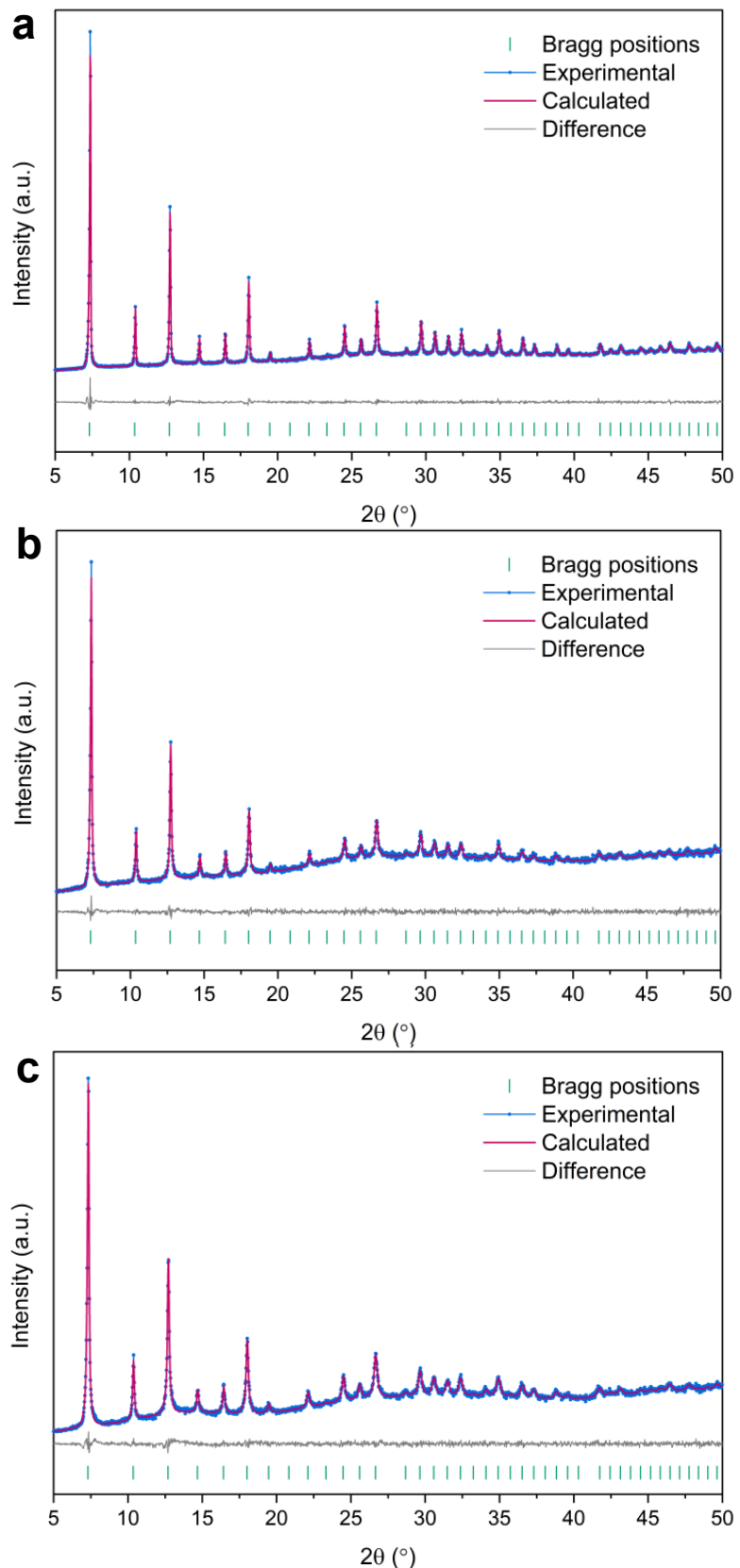


Figure S58. Pawley refinement of the, **a.** $(\text{ZIF-8})_{0.5}(\text{Inorganic})_{0.5}$, **b.** $(\text{ZIF-8})_{0.6}(\text{Inorganic})_{0.4}$ composite and **c.** $(\text{ZIF-8})_{0.7}(\text{Inorganic})_{0.3}$ composites.

Table S10. Pawley refinement details for 50-70% ZIF-8 composites. Space group for all samples was $I-43m$ and literature lattice parameter, $a = 16.8509(3)$ Å.¹ Experimental Lattice parameter of pristine ZIF-8 $a = 17.032(1)$ Å.

Sample	R_{wp}	Zero-point error	Profile parameters	Lattice parameter a (Å)
(ZIF-8) _{0.5} (Inorganic) _{0.5}	4.58%	0.02(7)	U: -0.33(9) V: 0.124(18) W: -0.007(2)	17.027(2)
(ZIF-8) _{0.6} (Inorganic) _{0.4}	4.29%	0.015(190)	U: -0.93(210) V: -0.01(43) W: -0.01(2)	17.025(4)
(ZIF-8) _{0.7} (Inorganic) _{0.3}	4.39%	0.005(210)	U: -0.1(26) V: -0.2(5) W: 0.002(250)	17.031(5)

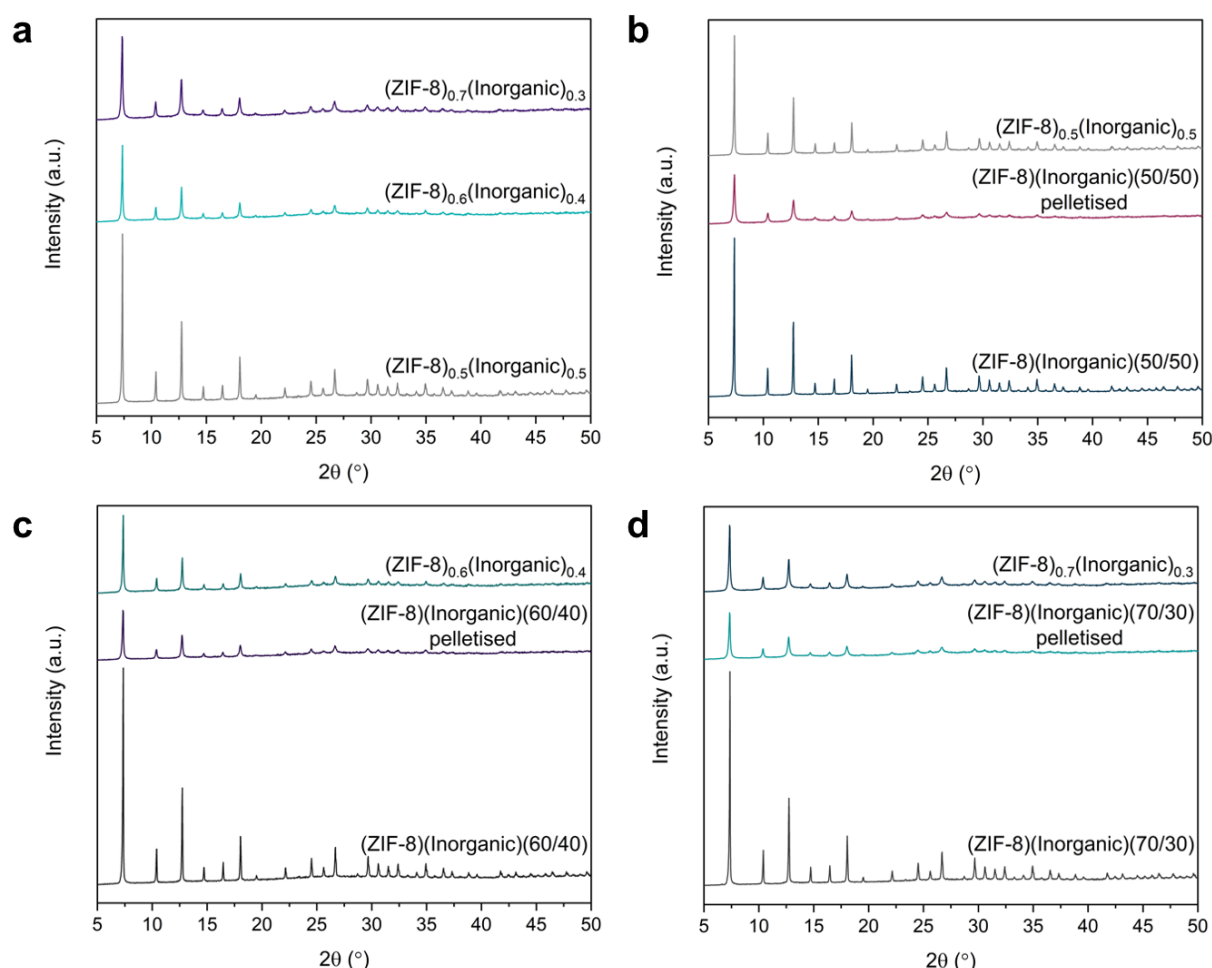


Figure S59. PXRD patterns of the, **a.** 50-70 wt% composites, **b.** 50 ZIF-8 wt% samples, **c.** 60 ZIF-8 wt% samples and **d.** 70 ZIF-8 wt% samples.

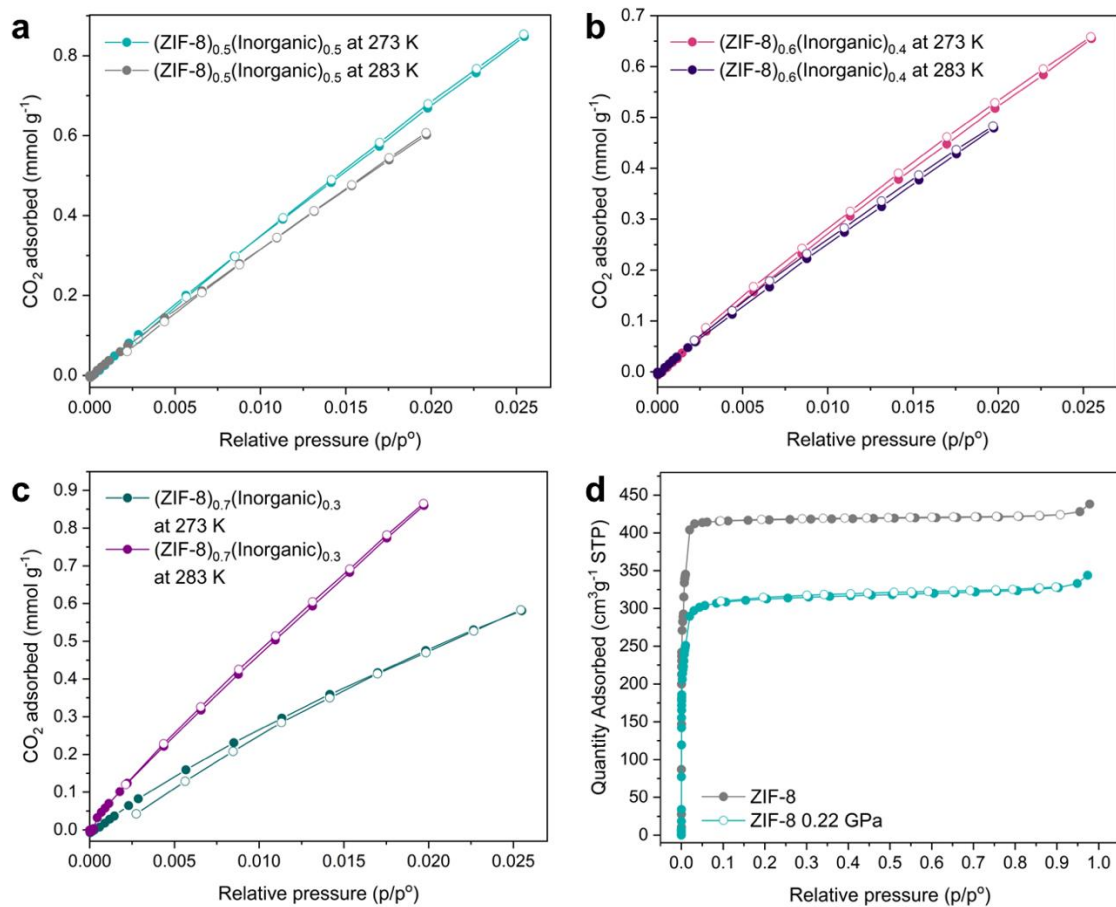


Figure S60. CO₂ isotherms at 273 and 283 K for **a.** (ZIF-8)_{0.5}(Inorganic)_{0.5} composite, **b.** (ZIF-8)_{0.6}(Inorganic)_{0.4} composite, **c.** (ZIF-8)_{0.7}(Inorganic)_{0.3} composite and **d.** N₂ isotherms at 77 K for ZIF-8 and ZIF-8 pelletised at 0.22 GPa. Open and closed circles indicate adsorption and desorption respectively.

Table S11. Maximum N₂ adsorbed (at relative pressure of 0.98) and multi-point BET surface area of the 50-70 wt% composites and ZIF-8 controls.

Sample	Quantity adsorbed (cm ³ g ⁻¹)	Quantity adsorbed (cm ³ per g MOF)	S _{BET} (m ² g ⁻¹)
Pristine ZIF-8	438	438	1867
ZIF-8 pelletised 0.22 GPa	344	344	1318
(ZIF-8) _{0.5} (Inorganic) _{0.5}	144.9	290	503
(ZIF-8) _{0.6} (Inorganic) _{0.4}	106.1	177	327
(ZIF-8) _{0.7} (Inorganic) _{0.3}	190.8	276	628

4.11 VT-PXRD of $(\text{ZIF-8})_{0.5}(\text{Inorganic})_{0.5}$ composite

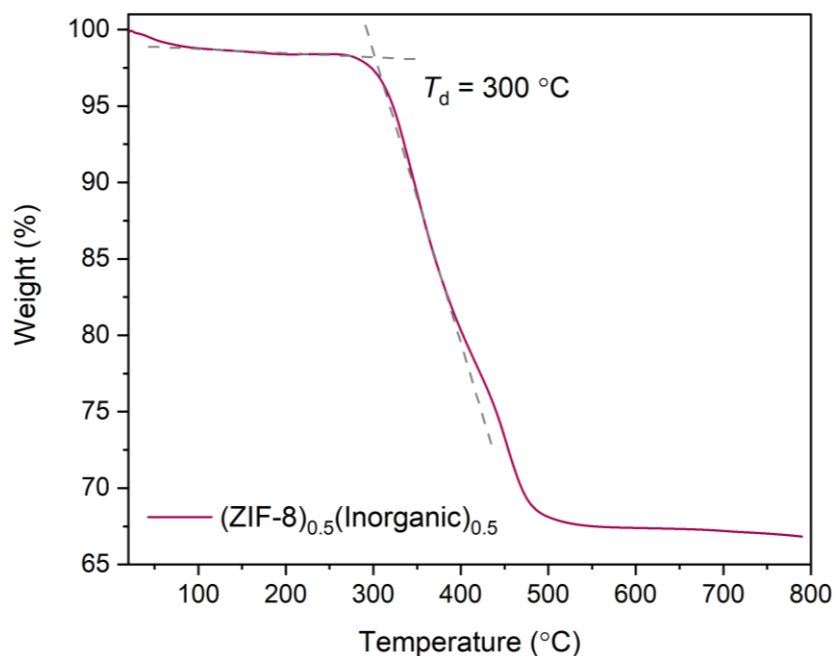


Figure S61. TGA trace of the $(\text{ZIF-8})_{0.5}(\text{Inorganic})_{0.5}$ composite, showing a T_d of $300 \text{ } ^\circ\text{C}$.

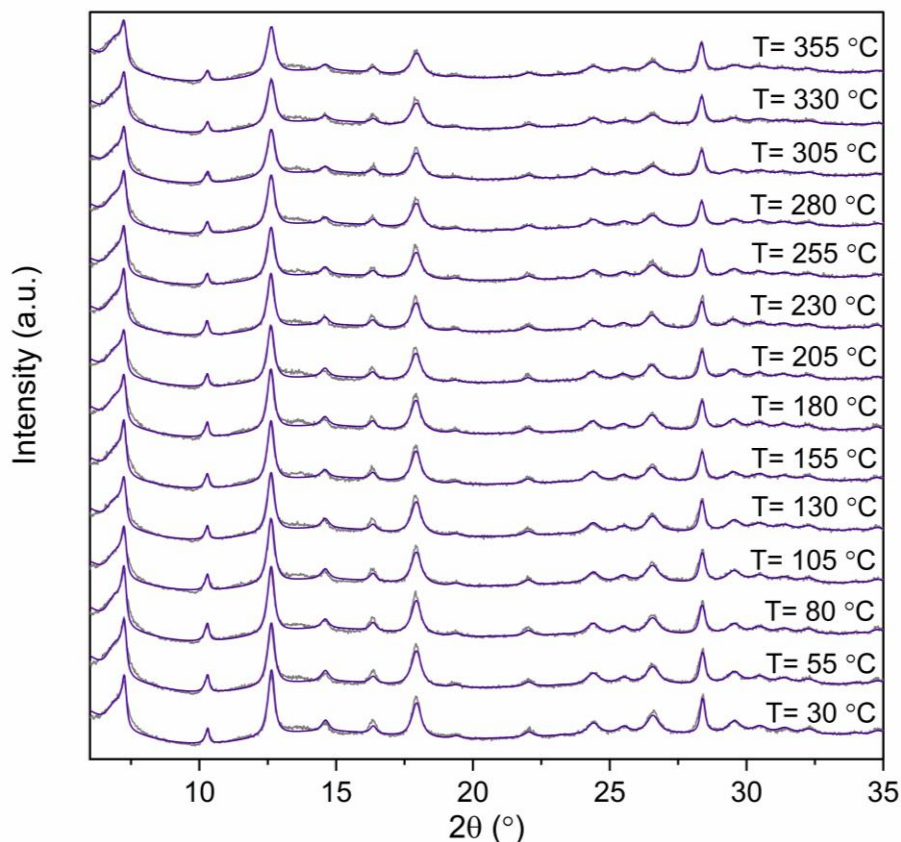


Figure S62. VT-PXRD output data for the ZIF-8 control from $30\text{-}355 \text{ } ^\circ\text{C}$. Experimental data are in purple, refinement data are in grey.

Table S12. Rietveld refinement values obtained from VT-PXRD data of the ZIF-8 control.

T (°C)	R _{wp}	χ ²	Lattice parameter a (Å)	Unit cell volume (Å ³)
30	7.487	2.128	17.072(4)	4975(4)
55	7.2	2.039	17.077(4)	4980(4)
80	7.244	2.043	17.073(4)	4976(4)
105	7.098	1.98	17.076(5)	4979(4)
130	6.967	1.93	17.072(4)	4976(4)
155	7.049	1.945	17.085(5)	4987(4)
180	7.165	1.983	17.088(5)	4990(4)
205	7.396	1.998	17.091(5)	4993(4)
230	6.84	1.865	17.083(5)	4986(4)
255	7.234	1.954	17.074(5)	4978(4)
280	6.824	1.844	17.071(5)	4975(4)
305	6.737	1.797	17.064(5)	4969(5)
330	6.682	1.793	17.068(5)	4972(5)

VT-PXRD analysis on the ZIF-8 control shows no loss in Bragg peak intensity of the ZIF-8 peaks for the entire temperature range, suggesting a lack of sample decomposition with respect to any changes observed (**Figure S62**). Negligible changes occur between 30 and 130 °C, after which the unit cell volume changes by 0.33 % up to 205 °C. After 205 °C, the cell volume decreases. This is in contrast to VT-PXRD data previously collected on pristine ZIF-8, where the framework increases ($\alpha_a = 9.21 \times 10^{-6} \text{ K}^{-1}$) from 200-500 °C.⁷

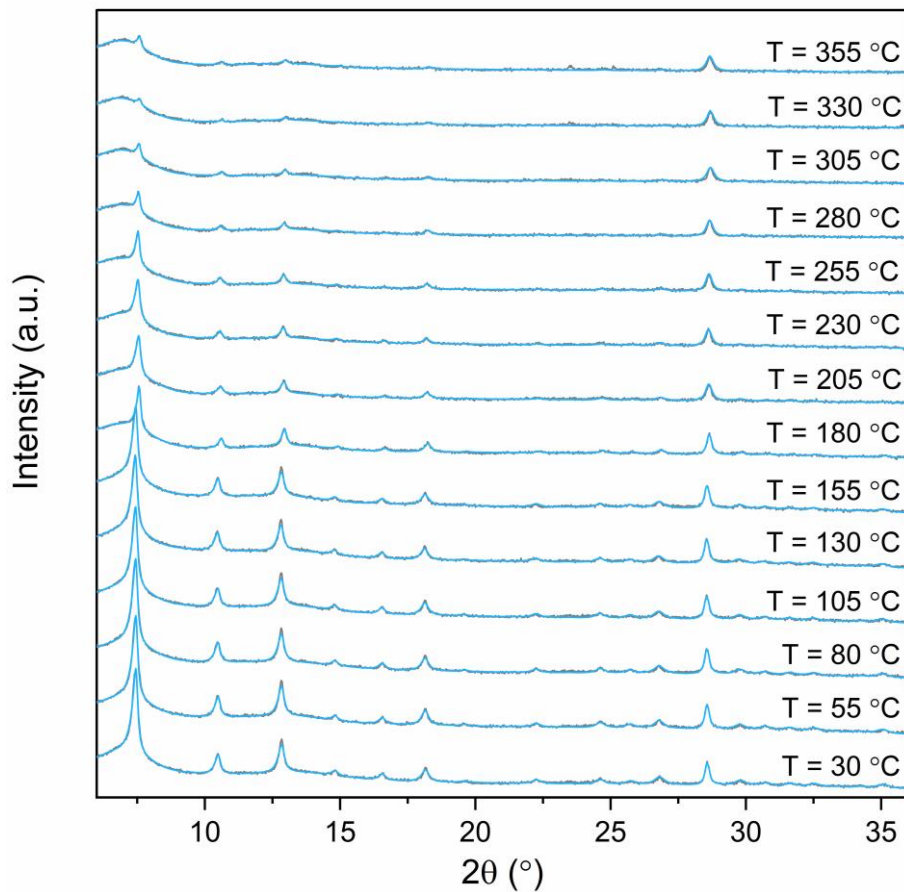


Figure S63. VT-PXRD output data for the $(\text{ZIF-8})_{0.5}(\text{Inorganic})_{0.5}$ from 30-355 °C. Experimental data are in blue, refinement data are in grey.

Apparent losses in peak intensity can be caused by specimen displacement, at least in part. In order to extract accurate unit cell parameters, the effect of specimen displacement on ZIF-8 peak positions was accounted for by fitting the calculated Si internal standard peak ($2\theta \sim 28.45^\circ$) position according to its thermal expansion equation (**Figure S63**).

Table S13. Rietveld refinement values obtained from VT-PXRD data of the $(\text{ZIF}-8)_{0.5}(\text{Inorganic})_{0.5}$ composite.

T (°C)	R_{wp}	χ^2	Lattice parameter a (Å)	Unit cell volume (Å ³)
30	5.335	1.572	17.040(3)	4948(3)
55	5.148	1.54	17.045(3)	4952(2)
80	5.176	1.528	17.049(3)	4956(2)
105	5.191	1.524	17.052(3)	4958(3)
130	5.018	1.477	17.059(3)	4965(3)
155	5.039	1.441	17.057(3)	4963(3)
180	5.068	1.255	17.040(3)	4948(3)
205	5.411	1.258	17.046(5)	4953(4)
230	5.577	1.28	17.055(5)	4961(4)
255	5.616	1.249	17.069(5)	4973(4)
280	5.838	1.236	17.076(6)	4979(5)
305	6.42	1.31	17.096(8)	4997(7)
330	6.531	1.281	17.057(10)	4962(9)
355	6.432	1.304	17.045(9)	4952(8)

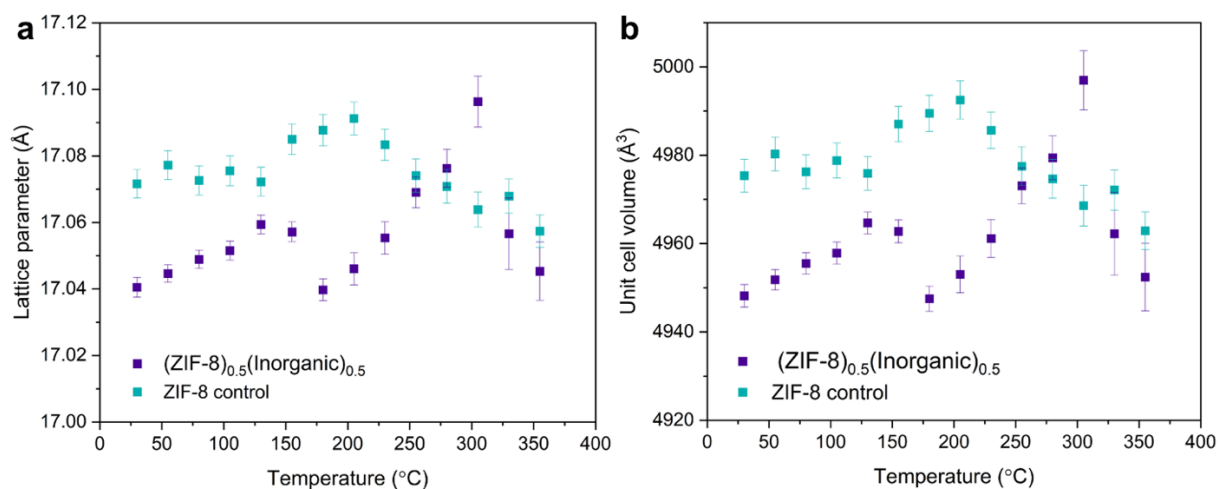


Figure S64. **a.** Refined lattice parameter of the $(\text{ZIF}-8)_{0.5}(\text{Inorganic})_{0.5}$ composite and ZIF-8 control and **b.** Refined unit cell volume of the $(\text{ZIF}-8)_{0.5}(\text{Inorganic})_{0.5}$ composite and ZIF-8 control.

Table S14. Calculated linear coefficient of thermal expansion of the $(\text{ZIF-8})_{0.5}(\text{Inorganic})_{0.5}$ composite.

Temperature range	Adj R^2	Slope*	α_a
30-130 °C	0.961	1.787×10^{-4}	$10.5 \times 10^{-6} \text{ K}^{-1}$
180-280 °C	0.985	3.757×10^{-4}	$22 \times 10^{-6} \text{ K}^{-1}$

* The calculated slope refers to the gradient of temperature *versus* lattice parameter graph, i.e., change in unit cell length *versus* temperature.

References

1. W. Morris, C. J. Stevens, R. E. Taylor, C. Dybowski, O. M. Yaghi and M. A. Garcia-Garibay, *J. Phys. Chem. C*, 2012, **116**, 13307–13312.
2. P. K. Jha, O. P. Pandey and K. Singh, *J. Mol. Struct.*, 2015, **1083**, 278–285.
3. Z. Huang, J. Zhou, Y. Zhao, H. Cheng, G. Lu, A. W. Morawski and Y. Yu, *Journal of Materials Research*, 2021, **36**, 602–614.
4. C. Hao, D. Zhou, J. Xu, S. Hong, W. Wei, T. Zhao, H. Huang and W. Fang, *J Mater Sci*, 2021, **56**, 9434–9444.
5. S. Tanaka, K. Fujita, Y. Miyake, M. Miyamoto, Y. Hasegawa, T. Makino, S. Van der Perre, J. Cousin Saint Remi, T. Van Assche, G. V. Baron and J. F. M. Denayer, *J. Phys. Chem. C*, 2015, **119**, 28430–28439.
6. A. M. Chester, C. Castillo-Blas, R. Sajzew, B. P. Rodrigues, R. Mas-Balleste, A. Moya, J. E. Snellson, S. M. Collins, A. F. Sapnik, G. P. Robertson, D. J. M. Irving, L. Wondraczek, D. A. Keen and T. D. Bennett, *Chem. Sci.*, 2023, **14**, 11737–11748.
7. Thomas Douglas Bennett, PhD thesis, University of Cambridge, 2012.